Realia et naturalia

DISSERTATIONES
PHYSICAE
UNIVERSITATIS
TARTUENSIS
96

MARTIN VILBASTE

Uncertainty sources and analysis methods in realizing SI units of air humidity in Estonia

DISSERTATIONES PHYSICAE UNIVERSITATIS TARTUENSIS
96

DISSERTATIONES PHYSICAE UNIVERSITATIS TARTUENSIS
96

MARTIN VILBASTE

Uncertainty sources and analysis methods in realizing SI units of air humidity in Estonia

UNIVERSITY OF TARTU
PRESS
1632

This study was carried out at the University of Tartu and the Centre for Metrology and Accreditation (MIKES).

The dissertation was admitted on December 4, 2014 in partial fulfilment of the requirements for the degree of Doctor of Philosophy in Physics, and was allowed for defence by the Council of the Institute of Physics, University of Tartu.

Supervisors: DSc Martti Heinonen, Centre for Metrology and Accreditation (MIKES), Espoo, Finland

PhD Olev Saks, University of Tartu, Tartu, Estonia

PhD Ivo Leito, University of Tartu, Tartu, Estonia

Opponent: PhD Vito Fernicola, National Institute of Metrological Research (INRiM), Turin, Italy

Defence: January 29, 2015, at the University of Tartu, Tartu, Estonia

ISSN 1406-0647
ISBN 978-9949-32-743-0 (print)
ISBN 978-9949-32-744-7 (pdf)

University of Tartu Press
www.tyk.ee

CONTENTS

LIST OF ORIGINAL PUBLICATIONS 7

AUTHOR'S CONTRIBUTION 7

ABBREVIATIONS 8

1 INTRODUCTION 9
1.1 Background 9
1.2 Objectives and progress in this work 10

2 LITERATURE OVERVIEW 12
2.1 Air humidity 12
2.2 Different air humidity measurement and calibration methods 13
2.3 Traditional GUM method for estimating uncertainties 18
2.4 Monte Carlo Method for uncertainty estimation 19
2.5 GUM modified by Bayesian approach 20
2.6 Construction of humidity generators 21
2.7 Uncertainty sources of dew-point generators 22
2.7.1 Overview 22
2.7.2 The effect of contaminated water on the dew-point temperature generation 23
2.7.3 The effect of moisture sorption and back-diffusion in trace moisture region 23
2.8 Uncertainty sources of the secondary standard of air humidity 24

3 MODELING AND EXPERIMENTAL 27
3.1 Set-up of Estonian air humidity reference standard 27
3.2 Uncertainty estimation for the reference values of relative humidity using the secondary standard 28
3.2.1 Mathematical model for the relative humidity reference value 28
3.2.2 Estimation of standard uncertainty components for air temperature and dew-point temperature 31
3.3 The study of contaminated water on the dew-point temperature generation 32
3.3.1 Experimental set-up for studying the effect of contaminated water in a saturator 32
3.3.2. Performance of the set-up 34
3.3.3. Measurement of the amount of natural contamination 36
3.3.4 Calculation of the effect of natural contamination on the dew-point temperature generation 37
3.3.5 Different calculation methods for ionic contamination of water 38

3.4 Study of leaks in the sampling line in the trace moisture region 38
3.4.1 Experimental set-up and description of measurements..... 38
3.4.2 Calculation of the critical flow-rate of air through the leak hole 40

4 RESULTS AND DISCUSSION 44
4.1 Uncertainty estimation for the relative humidity reference value using the secondary standard of humidity..... 44
4.1.1 Comparison of uncertainties using three approaches..... 44
4.1.2 The stability of the chilled mirror hygrometer..... 46
4.1.3 Interlaboratory comparisons 47
4.2 The effect of water contamination on the dew-point temperature generation..... 49
4.3 The effect of leaks in a sampling line on the dew-point temperature of air 54
4.4 Possible future development of Estonian reference standard of air humidity..... 55

5 CONCLUSIONS..... 57

6 SUMMARY 59

7 SUMMARY IN ESTONIAN 61

8 APPENDIX 1 63

9 REFERENCES..... 65

ACKNOWLEDGEMENT..... 70

PUBLICATIONS 71

CURRICULUM VITAE 104

ELULOOKIRJELDUS..... 106

LIST OF ORIGINAL PUBLICATIONS

I M. Vilbaste, G. Slavin, O. Saks, V. Pihl, I. Leito. Can coverage factor 2 be interpreted as an equivalent to 95% coverage level in uncertainty estimation? Two case studies. *Measurement*, **2010**, 43(3), 392–399.

II M. Vilbaste, M. Heinonen, O. Saks, I. Leito. The effect of water contamination on the dew-point temperature scale realization with humidity generators. *Metrologia*, **2013**, 50, 329–336.

III M. Heinonen, M. Vilbaste. Frostpoint measurement error due to a leak in a sampling line. *International Journal of Thermophysics*, **2008**, 29(5), 1589–1597.

AUTHOR'S CONTRIBUTION

I Development of the calculation methods; conducting all calculations; analysis of the results; main part of the text of the article.

II Development of the measurement models and methods; design of the experiments; conducting most of the experiments; analysis of the measurement results; main part of the text of the article.

III Development of the calculation methods; performing part of the measurements, performing part of the analysis of the measurement results.

ABBREVIATIONS

NMI – National Metrology Institute
CMH – Chilled mirror hygrometer
PDF – Probability density function
PRT – Platinum resistance thermometer
GUM – Guide to the Expression of Uncertainty in Measurement
MCM – Monte Carlo method
TOC – Total organic carbon
MDFG – MIKES dew/frost-point generator

1 INTRODUCTION

1.1 Background

Modern society needs accurate measurements in many fields of activity. Well functioning metrological system helps developing industry in the country and to create healthier and safer living conditions for inhabitants. The national standards (etalons) are maintained, developed and disseminated by National Metrology Institutes (NMI) that also provide expertise in appropriate fields of measurement. While the first NMIs emerged just after signing the Metre Convention treaty in 1889 [1], Estonia began to develop its national standards only in the beginning of 1990s. As in many countries, in Estonia designated institutes (DI) are also involved in maintaining and developing measurement standards and disseminating relevant units.

In 2002 the Phare Project called "Development of Conformity Assessment Infrastructure in the Field of Metrology" was initiated [2]. This project offered help for developing Estonian present national standards of mass and length further. It also helped Estonia to establish national standards of temperature and electrical quantities (direct voltage and resistance) at AS Metrosert as well as air humidity, air velocity and liquid chromatography-mass spectrometry (LCMS) standards at the University of Tartu and surface roughness standard at the Tallinn University of Technology. In 2004 the necessary apparatus for setting up the standards arrived in Estonia and Estonian specialists were trained by Finnish experts. In 2010 the air humidity and air velocity standards were named Estonian reference standards according to the governmental decree.

Air humidity is an important parameter that affects many aspects of life. Humidity must be controlled and measured in museums, libraries, semi-conductor and food industries, pharmaceutical enterprises. It affects human thermal comfort and is an important parameter in weather forecasting [3].

The demand on the accuracy of humidity measurements is increasing and more accurate hygrometers for measuring air humidity are being produced. It is therefore important to develop calibration methods and reduce measurement uncertainties associated with the calibration methods. Testing Centre of University of Tartu has developed secondary standard of air humidity. This standard is based on the chilled mirror hygrometer in the climatic chamber. This calibration method is rather flexible and convenient to use but the measurement uncertainties are higher than in the case of humidity generators that have been set up by many NMIs of industrial countries. Although at the present moment the secondary standard of air humidity meets the requirements of Estonia it is still reasonable to develop it further to meet the future needs.

It is necessary to generate and measure the humidity of very dry gases for several kinds of manufacturing processes. At very low humidities the effect of leaks in the tubing can lead to significant errors in dry gas generation and its humidity measurement. It may be necessary to extend the air temperature range

of the present secondary standard of air humidity towards higher air temperatures in order to be able to perform standard tests for electronic products at 85 °C and calibrate relative humidity sensors at higher air temperatures. It may turn out to be useful in future to construct a dew-point generator that covers significantly larger dew-point temperature range than the present simplified single-pressure dew-point generator. Such a generator could be useful for calibration of chilled mirror hygrometers. It would also be possible to calibrate the standard chilled mirror hygrometer in site and thereby eliminating potential risks in sending the hygrometer for calibration to foreign NMIs.

1.2 Objectives and progress in this work

In metrology it is very useful to carry out measurements and calculations using different methods and compare the results to each other. This helps to reveal systematic errors in the measurement procedure and detect potential effects of correlations between input quantities. For this reason the uncertainty estimation of the relative humidity reference value of Estonian reference standard of humidity was carried out using three methods [**I**]. These were the traditional GUM method, the Monte Carlo Method (MCM) and the GUM method modified by the Bayesian approach. The expanded uncertainties calculated by the three methods were found to agree within 0.04 %rh at medium and high relative humidity cases [**I**].

A simplified single pressure dew-point generator for working in the limited dew-point temperature range of 14 °C to 19 °C was constructed in order to check the performance of the reference chilled mirror hygrometer between its calibrations at foreign NMIs and detect the possible effects of transportations. This increases the reliability of dew-point temperature measurements in Estonia. Performance tests were carried out for the simplified dew-point generator.

The expanded uncertainties of dew-point generators are becoming smaller in time. Therefore it is increasingly important to estimate also uncertainty components that were believed to be negligible in the past. These uncertainty sources include the effect of contaminated water in the saturator of humidity generator as well as the effect of potential leaks in the sampling line. Investigation and quantification of the influence of these effects is the central aim of this thesis. This knowledge will also be needed when developing Estonian air humidity standard further.

The dew-point temperature drop due to contamination of water samples was studied in the context of humidity generators [**II**]. The water samples were kept in closed and ventilated vessels made of different materials for 2 months and 13 months periods. In all the cases the calculated dew-point temperature drop due to contamination of the water samples was found to be below 0.1 mK [**II**]. In addition, the dew-point temperature drop due to contamination was directly measured and compared to estimates obtained using three calculation methods.

The results agreed well, and the widely used Raoult's law was found to be a sufficient method for calculating water-vapour pressure drops due to contaminated water in the saturator unit of dew-point generator [**II**].

The effect of leaks in the sampling line may be one of the major uncertainty contributions at very low frost-point temperatures even if pressure in the sampling line exceeds ambient pressure [4]. Tiny holes with different diameters were drilled inside the wall of the tubing in order to study the effect of leaks. It was found that certain critical flow-rates of dry air through the leak hole practically stopped the back-diffusion of water molecules into the tubing [**III**]. The results of calculations and direct measurements of the critical flow-rate agreed well at frost-point temperature $T_f = -80$ °C [**III**]. The experiments with loosened Swagelok and VCR connectors showed that the latter is more sensitive to back-diffusion of water molecules [**III**].

2 LITERATURE OVERVIEW

2.1 Air humidity

Air humidity, i.e. the content of water-vapour in air, can be characterized by several quantities. The most widespread air humidity quantities are absolute humidity, mixing ratio, amount fraction, relative humidity and dew-point temperature.

Absolute humidity D_w is water-vapour density of air (g/m^3). Mixing ratio r_w is defined as the ratio of the mass of water-vapour to the mass of air from which the water-vapour has been entirely removed (g/kg). [5].

The amount fraction of water-vapour x_w is defined as the number of water-vapour moles n_w to the number of moist air moles in a given air volume:

$$x_w = \frac{n_w}{n_w + n_{da}}, \tag{2.1}$$

where n_{da} is the number of dry air moles. Amount fraction as well as mixing ratio do not depend on air temperature and pressure.

For many practical applications it is necessary to know whether condensation will take place when air gets in contact with colder surfaces. In these cases, it is necessary to know the dew-point temperature of air. For any given moisture content of air there is a certain temperature at which there is thermodynamic equilibrium between water-vapour and liquid water or ice. This temperature is called either the dew-point temperature of air T_d or frost-point temperature T_f depending on whether condensation takes place in the form of water droplets or ice crystals, respectively. The actual water-vapour pressure at air temperature e_w is equal to the saturated water-vapour pressure at dew-point temperature or the saturated water-vapour pressure at frost-point temperature:

$$e_w\Big|_{p,T} = f_w(p,T_d)\cdot E_w(T_d) = f_i(p,T_f)\cdot E_i(T_f), \tag{2.2}$$

where $E_w(T_d)$ and $E_i(T_f)$ are the saturated vapour pressures of pure water and ice, respectively. In equation (2.2) $f_w(p,T_d)$ and $f_i(p,T_f)$ are the corresponding enhancement factors depending on air pressure and dew-point temperature or frost-point temperature values. Enhancement factor f is defined by mole fraction using the following formula:

$$f = \frac{x_w \cdot p}{E_w}. \tag{2.3}$$

It takes the interaction between dry air and water-vapour molecules into account. Based on experimental results and thermodynamic modeling, formulae for calculation of enhancement factor have been proposed in [6,7].

It is important to know whether condensate below 0 °C is in the form of supercooled water or ice. It is known that the water-vapour pressure above supercooled water exceeds the water-vapour pressure above ice at the same temperature. Therefore frost-point temperature T_f is higher than dew-point temperature T_d corresponding to the same air humidity.

Relative humidity h is the ratio of actual water-vapour pressure e_w to the saturated water-vapour pressure E'_w at the same air temperature T and pressure p:

$$h = \frac{e_w}{E'_w}\Big|_{p,T} \cdot 100\% = \frac{f(p,T_d)\cdot E_w(T_d)}{f(p,T)\cdot E_w(T)} \cdot 100\% \quad (2.4).$$

Since enhancement factor depends weakly on temperature it is possible to omit the enhancement factors in equation (2.4) in many practical cases.

2.2 Different air humidity measurement and calibration methods

There are several principles known for measurement of air humidity. Nowadays the most widespread instruments are impedance hygrometers, condensation dew-point hygrometers and psychrometers. Other working principles of hygrometers include dimensional change of moisture absorbing materials, spectroscopy [8], etc. The non-exhaustive classification of hygrometers according to the working principle is presented on Figure 1 below.

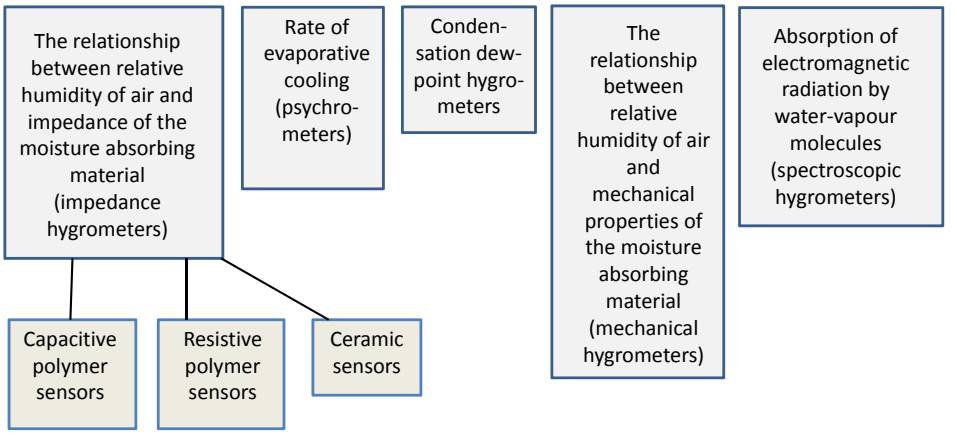

Figure 1 The most common working principles of hygrometers

The working principle of impedance hygrometers is based on the relationship between relative humidity of air and dielectric permittivity or resistance of a moisture absorbing material.

Capacitive polymer sensors are nowadays very popular due to the broad relative humidity measurement range (2 %rh to 100 %rh), moderate accuracy, compact size and relatively low cost. Capacitive hygrometers also perform very fast. However, the sensors of capacitive hygrometers are sensitive to contamination and their response is dependent on ambient temperature. Nowadays automatic compensation for the temperature dependence of sensors has been applied to the capacitive hygrometers. Capacitive hygrometers measure low relative humidities better than high relative humidities [9].

Resistive hygrometers on the other hand perform better in the high relative humidity range. The measurement range of relative humidity is between 15 %rh and 99 %rh [9]. The other good properties of resistive humidity sensors include fast response, compact size, moderate accuracy and low cost. Unfortunately, resistive hygrometers do not stand direct contact with water.

A general disadvantage of impedance hygrometers is related to significant long-term drift and hysteresis. Therefore it is necessary to calibrate resistive hygrometers as well as capacitive hygrometers in a shorter time interval than other types of hygrometers [10].

Psychrometer is a device that measures the temperature difference between dry and wet thermometers. This temperature difference is related to relative humidity at the measurement location. If the relative humidity of air is low then the temperature difference is high due to high evaporative cooling. In modern psychrometers, liquid-in-glass thermometers have been replaced by electrical thermometers to measure the temperature difference. Psychrometers are accurate measuring instruments if operated correctly. It must be checked that the wick around the wet thermometer is clean and it does not disturb air movement across the thermometers. Also the speed of air flow across the thermometers must be sufficiently high. It is not correct to measure with psychrometers in small enclosures because water evaporation from the wick of the wet thermometer will increase the air humidity content in the enclosure. The measurement of relative humidities lower than 15 %rh is accompanied by higher errors [9] than the typical error of about 2 %rh. This can be explained by parasitic heat flows because often the dry and wet bulb thermometers are not isolated from each other well enough. Furthermore, the properties of the wick and possible air flow anomalies around the wet bulb thermometer become more important for higher evaporation rates.

The operation principle of the condensation dew-point hygrometer is shown on Figure 2. It is based on the zero net mass transfer of water molecules between the condensed layer and moving air. Constant dew or frost layer is maintained on the mirror surface of the condensation dew-point hygrometer (chilled mirror hygrometer) by controlling the mirror temperature. The temperature of the condensate on the mirror surface can be treated as the dew-

point temperature (or frost-point temperature) of air flowing over the mirror. The temperature of the plated copper mirror that is assumed to be at almost the same temperature as the condensate is measured with platinum resistance thermometer imbedded in the mirror. The temperature of the mirror is controlled by a Peltier cooler and an electro-optical feedback.

There are several effects influencing the accuracy of the chilled mirror hygrometer (CMH). The mirror of the hygrometer should be kept clean because dissolved contaminants on the mirror will cause the mirror temperature to rise due to the Raoult's law. For this reason it is necessary to clean the mirror surface regularly. Since contamination of the mirror is a progressive process it is necessary to use the balance compensation option of the chilled mirror hygrometer before measurements. During balancing the mirror of the hygrometer is heated so that condensation layer evaporates from it leaving only contamination on the mirror. Thus it is possible for the system to compensate for the reduced light intensity due to contamination on the mirror. For reference and calibration laboratories it is better to initiate the balancing of the hygrometer manually but for industrial applications it is reasonable to use automatic balance control [9].

According to the Kelvin effect the water-vapour pressure above tiny water droplets is higher than above a planar surface of water. This effect lowers the reading of the CMH. The Kelvin effect is usually rather small (5 mK or less depending on the droplet size). The other uncertainty sources are related to measurement of the temperature of the condensate layer on the CMH mirror (heat conductance between the mirror surface and the PRT as well as between the mirror surface and the condensate layer, error of the PRT, etc.).

When measuring dew-point temperatures below 0 °C it is sometimes difficult to determine whether the mirror is covered with ice crystals or droplets of supercooled water. The most widespread method to overcome this is to equip a chilled mirror sensor with a microscope or camera for visual observation. A wrong decision may cause remarkable errors because the water-vapour pressure above supercooled water exceeds the water-vapour pressure above ice. The difference between frost-point temperature and dew-point temperature at –38 °C dew-point temperature is about 3.4 °C.

All in all, CMHs are very accurate and reliable air humidity measuring devices with accuracy about ± 0.1 °C dew-point temperature. The corresponding error in relative humidity at room temperature does not exceed 0.6 %rh. Unfortunately, CMHs are very expensive measuring instruments and perform rather slowly, especially in the lower dew-point temperature range.

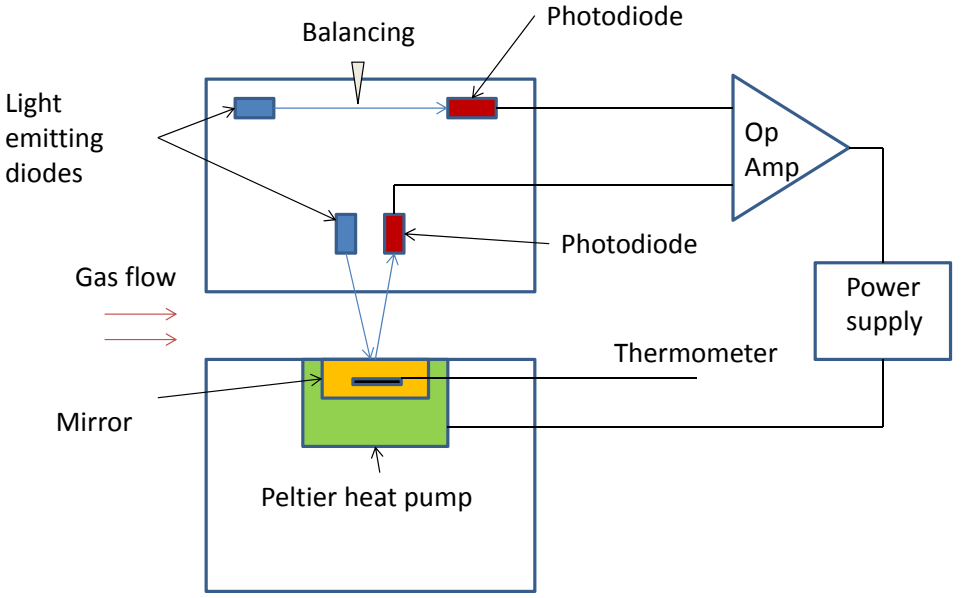

Figure 2 Working principle of chilled mirror hygrometer

It is necessary to periodically calibrate hygrometers in order to minimize the measurement bias and to ensure that their readings are traceable to the SI units. Usually calibration of measuring instruments is performed by calibration laboratories that acquire their traceability via NMIs or Reference standard laboratories.

The most accurate humidity standard is the gravimetric hygrometer but only in a limited range. In a mid-humidity range, a gravimetric hygrometer can be about ten times more accurate than humidity generators [11]. It measures the mixing ratio of air or nitrogen by weighing the amount of water that has been absorbed by a desiccant or a cold trap and by measuring the mass of dry gas. Unfortunately, gravimetric hygrometers are not practical in everyday use being expensive and complicated [12]. A good accuracy can only be achieved with a long measurement time and a stable humidity generator. Gravimetric hygrometers are used in a few NMIs in order to test the performance of humidity generators [13].

The main practical possibilities for calibrating hygrometers are to use different types of humidity generators, saturated salt solutions and climatic chambers combined with accurate hygrometers [8,9].

The simplest generator is a single pressure dew-point generator in which air is forced to move above the plain surface of water or ice and ideally becomes saturated with respect to water or ice at the same temperature that is equal to the dew-point temperature of air leaving the generator.

In the case of two-temperature humidity generator air saturated with respect to water or ice flows into a measurement chamber at a temperature higher than

the saturation temperature. By varying the temperature of the saturator and/or the measurement chamber it is possible to obtain a chosen relative humidity value at a chosen temperature.

In the case of two-pressure humidity generator air is saturated at a higher pressure and expanded to a lower pressure. Adjustment of the pressures in the saturator and/or the measurement chamber enables to obtain a chosen dew-point temperature or relative humidity value. Two-pressure generators operate faster than two-temperature generators because the stabilization of temperature in the liquid bath and in the measurement chamber takes more time than adjustment of pressure. Two-temperature generators on the other hand are slightly more accurate because the pressure measurement uncertainty is lower [14]. Furthermore, at higher pressures the enhancement factor uncertainty may have a high contribution to the overall uncertainty of a two-pressure generator. The results of an extensive key comparison show that the lowest dew-point temperature standard uncertainties vary from 0.01 K to 0.02 K in the dew-point temperature range of –50 °C to +20 °C [15].

Two-flow humidity generator makes use of the controlled flow-rates of dry air and moist air that are mixed together to obtain a chosen value of humidity in the measurement chamber. It is not as accurate method as the two-temperature and the two-pressure methods due to additional uncertainties that are related to flow measurements. Similar to the two-pressure generator the two-flow generator operates fast. Two-pressure humidity generators and two-flow generators can both be used for the generation of dew-point temperature and relative humidity values.

In the case of a diffusion tube humidity generator water molecules from the diffusion cell diffuse into the stream of dry gas to generate air with chosen humidity [16]. This method is used for generating gas with very low humidity (trace moisture). In most accurate systems the diffusion rate is determined by weighing using a suspension balance. Determination of carrier gas flow-rate has a significant effect on the final uncertainty.

Saturated salt solutions can be used to generate an environment of a particular relative humidity in an enclosed space. It is possible to obtain a wide range of relative humidity values by using different salts [17]. The principle of operation is based on the fact that different salts have different solubilities in water and the water-vapour pressure depression is proportional to the amount fraction of dissolved salt ions according to the Raoult's law. The saturated salt solution method is slow for calibrating relative humidity hygrometers that are also exposed to ambient conditions between each measurement points. The contamination of saturated salt solutions is potentially a significant error source because equilibrium relative humidity is sensitive to contaminants and the contamination risk is high due to practical realization.

2.3 Traditional GUM method for estimating uncertainties

It is very fundamental in physics that the true value of a measured quantity is unknown and it can only be estimated. The measurement uncertainty shows how well the estimate represents the true value. It is a non-negative parameter that characterizes the dispersion of values that could reasonably be attributed to the measurand [18].

The value of the output quantity or measurand y is calculated from input quantities x_i using the appropriate mathematical model f:

$$y = f(x_1, x_2, ..., x_n) \tag{2.5}$$

The standard uncertainties of input quantities $u(x_i)$ characterize the distribution of values of the input quantities and are expressed as standard deviations.
The combined standard uncertainty of y, $u_c(y)$, is evaluated from standard uncertainties of input quantities $u(x_i)$ by the following equation [19]:

$$u_c(y) = \sqrt{\sum_{i=1}^{n}\left[\frac{\partial f}{\partial x_i}\cdot u(x_i)\right]^2 + 2\cdot\sum_{i=1}^{n-1}\sum_{j=i+1}^{n}\frac{\partial f}{\partial x_i}\frac{\partial f}{\partial x_j}\cdot u(x_i)\cdot u(x_j)\cdot r(x_i,x_j)}\ , \tag{2.6}$$

where $\frac{\partial y}{\partial x_i}$ is the partial derivative of the measurand with respect to the input quantity x_i and $r(x_i, x_j)$ is the linear correlation coefficient between input quantities x_i and x_j.

Two different types of methods for evaluating standard uncertainty are introduced in the Guide to the Expression of Uncertainty in Measurement (GUM) [19]. The evaluation of type-A uncertainties is based on the statistical analysis of a series of measurements while the evaluation of type-B uncertainties is based on other means. However, no distinction between the methods is made when calculating the combined standard uncertainty u_c of a measurand y.

In most cases it is necessary to calculate the expanded uncertainty that encompasses large fraction of the values that can reasonably be attributed to the measurand. Quite often the approximate coverage probability $P = 95\%$ is used. In order to calculate the expanded uncertainty at a chosen coverage probability the combined standard uncertainty is multiplied by a suitable coverage factor k. If the measurand is normally distributed and the coverage probability is chosen to be approximately 95%, then the coverage factor $k = 2$ should be used to calculate the expanded uncertainty $U(y)$ via the combined standard uncertainty:

$$U(y) = 2 \cdot u_c(y) \tag{2.7}$$

If the measurement model is linear and all the input quantities are distributed normally the probability density function of the measurand is also a normal distribution. Furthermore, the assumption of normal distribution of the measurand is fulfilled even if the input quantities are not normally distributed, if the conditions of the Central Limit Theorem hold, i.e. there are several input quantities and none of them is dominating in the uncertainty budget. This condition is quite often fulfilled. However, if it is assumed that the measurand is distributed similarly to the Student's distribution then the Welch-Satterthwaite formula is used to calculate the effective number of degrees of freedom v_{eff} [19]. The combined standard uncertainty of the measurand is multiplied by the student's coefficient $t(v_{eff},P)$ for evaluating the expanded uncertainty at coverage probability P:

$$U(y) = t(v_{eff}, P) \cdot u_c(y) \tag{2.8}$$

Analytical expressions of combined standard uncertainty for the dew-point temperature [20–22] as well as for relative humidity and mixing ratio [21–22] have been derived for different types of humidity generators.

One problem with the GUM method is related to strongly nonlinear measurement models. It is troublesome to calculate higher order Taylor series components while evaluating combined standard uncertainty of the measurand. This drawback is related to humidity measurements because saturated water-vapour pressure is strongly non-linear with respect to temperature. Secondly, it is also difficult to determine correlations between input quantities. Thirdly, the traditional GUM method does not provide us with the probability density function (PDF) of the measurand making it impossible to know the correct value of the coverage factor in most of the cases. In principal it is possible to use the propagation of distributions to evaluate the PDF of the measurand but unfortunately these calculations can be carried out analytically only in the simplest cases and in most cases numerical methods have to be used [23]. Nowadays, the most widespread numerical method for evaluating the PDF of the measurand is the Monte Carlo Method (MCM).

2.4 Monte Carlo Method for uncertainty estimation

Joint Committee for Guides in Metrology (JCGM) has published Supplement 1 to the Guide to the Expression of Uncertainty in Measurement [24]. This Supplement is named as "Propagation of distributions using a Monte Carlo method". The essence of the MCM is the repeated sampling from PDFs of input quantities $\boldsymbol{X}$ and evaluation of the model to find y_i in each case. The index i counts the Monte Carlo trials. The distribution function $G_Y(\eta)$ encodes all the

necessary information about the measurand y (PDF, best estimate, standard deviation, coverage interval). The number of Monte Carlo trials M has to be sufficiently large (about 1 000 000) to get reliable PDF of the output quantity Y.

According to the results of several studies the MCM has broader applicability than the GUM uncertainty framework [23–29]. It works better than the GUM method if the measurement model is not linear and one or few non-normally distributed input quantities dominate in the uncertainty budget. In a study about estimating the uncertainties for the two-temperature humidity generator the GUM method and the MCM showed only small differences [30].

2.5 GUM modified by Bayesian approach

This approach saves one from calculating the effective number of degrees of freedom via the Welch-Satterthwaite formula.

In the traditional GUM method the type-A uncertainties are treated from classical viewpoint while the Bayesian approach is used to treat type-B uncertainties [31–33]. It is possible to use the Bayesian approach to estimate both types of uncertainties. In the traditional GUM method the type-A uncertainties are evaluated as a standard deviation of the mean:

$$u_A(x) = \sqrt{\frac{\sum_{i=1}^{n}(x_i - \bar{x})^2}{n \cdot (n-1)}} \qquad (2.9),$$

where n is the number of repeated measurements.

The Bayesian analogue of the type-A uncertainty is equal to the standard deviation of the scaled and shifted t-distribution [24,31–33].

$$u_{Bayes}(x_A) = \sqrt{\frac{n-1}{n-3}} \cdot u_A(x) \qquad (2.10).$$

The combined standard uncertainty is calculated according to the law of propagation of uncertainties (equation 2.6) and the type-A uncertainties are replaced by their Bayesian analogues. The Bayesian analogue of the type-A uncertainty saves us from problems related to low number of repeated measurements relevant to the traditional GUM method. The Bayesian analogue of the type-A uncertainty does not carry any degrees of freedom [33]. Therefore it can be assumed that the measurand is distributed approximately normally and the coverage factor k = 2 is used to calculate the expanded uncertainty at approximately 95 % confidence level.

2.6 Construction of humidity generators

In many NMIs humidity generators including dew-point generators serve as primary standards of air humidity [34–57]. The simplified construction of a single pressure dew-point generator is presented on Figure 3. The central part of the dew-point generator is a saturator unit that is immersed in a temperature controlled liquid bath. Air is forced to move above the plane surface of water or ice lying on the bottom of the saturator unit in a serpentine way in order to increase the time that air is in contact with water or ice. In an ideal saturator the dew-point temperature of air leaving the saturator is equal to the temperature in the saturator. Usually the pre-saturator lies before the saturator. Most of the condensation or evaporation will take place in the pre-saturator and in the following heat exchanger. So the final saturation is assumed to take place in the main saturator unit. The heat exchanger is usually a spiral of stainless steel pipe. The temperature of the liquid in the bath is usually measured with platinum resistance thermometers (PRTs). The pressure is also measured at the saturator unit and at the point of use. The liquid is constantly stirred in the bath.

It is important to keep the dew-point temperature of air entering the condensation based saturator higher than saturator temperature. In such a case the condensation will take place in the pre-saturator as well as in the heat exchanger and in the saturator unit. In the opposite case the evaporation from the pre-saturator and the saturator unit may not be high enough to fully saturate gas with respect to water. [37].

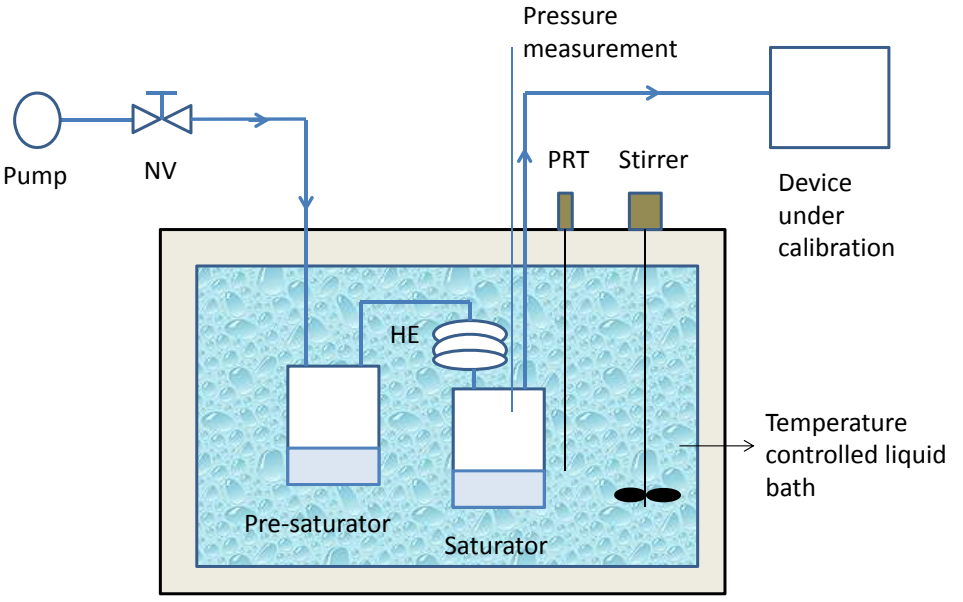

Figure 3 Simplified dew-point generator, NV – needle valve, HE – heat exchanger, PRT – platinum resistance thermometer

Single-pressure as well as two-pressure dew-point generators are often used to calibrate chilled mirror hygrometers. Air flow-rate that is used for calibrating chilled mirror hygrometers lies typically in the range 0.5 l/min to 1 l/min. In order to be able to calibrate more chilled mirror hygrometers at the same time the saturator must work effectively at higher air flow-rates. In the case of two-pressure dew-point generators the pressure is reduced to ambient pressure by using expansion valves or mass flow controllers.

A relative humidity generator is formed by combining a dew-point generator with a measurement chamber. In the case of two-temperature humidity generator the temperature of the measurement chamber has to be higher than air temperature in the saturator. For two-pressure humidity generators the pressure in the saturator must be higher than the pressure in the measurement chamber. Combinations of two-temperature and two-pressure humidity generators have been realized at several NMI-s [37,56–57].

The two-temperature and two-pressure humidity generator enables to generate same values of dew-point temperature by different pressure and temperature combinations [50]. This kind of consistency test makes the generated dew-point temperature values even more reliable because operating with different pressure and temperature combinations enables to get more independent repetitions of measurements which reduces the uncertainty when combining these different measurement results. It is important to heat the tubing between the saturator and the measurement chamber if the dew-point temperature exceeds ambient temperature in order to avoid condensation of water-vapour in the tubing.

2.7 Uncertainty sources of dew-point generators

2.7.1 Overview

In order to use a dew-point generator as a primary realization of a dew-point temperature scale it has to be thoroughly studied in order to detect and evaluate all significant uncertainty sources. The main sources of measurement uncertainty in dew-point generators are related to saturation efficiency, temperature measurements in the liquid bath and pressure measurements in the saturator as well as in the point of use [34–38,40,42–43,45,48,50,59].

A saturator should be efficient enough to fully saturate gas at all flow, pressure and temperature conditions used in calibrations [59]. The saturation efficiency can be studied by monitoring the difference between the saturator temperature and the dew-point temperature of air leaving the saturator while changing the flow-rate, temperature and water-vapour content of the inlet gas. Ideally the difference does not depend on the inlet parameters. In practice, the estimation of the uncertainty due to the saturation efficiency is limited by the capability of detecting changes in the efficiency.

The main sources of temperature measurement uncertainty are related to temperature inhomogeneity in the liquid bath, temperature instability in the liquid bath and uncertainty sources due to the thermometer itself (calibration uncertainty, resolution, long term drift, possible self-heating) [10].

The main sources of pressure measurement uncertainty are due to the pressure meter (calibration uncertainty, hysteresis, resolution, long term drift) and spatial distribution of air pressure in the saturator and the tubing.

The expanded uncertainties of different realizations of dew-point temperature vary between 0.02 °C to 0.06 °C in a wide range of temperatures [15]. At very low humidity values (trace moisture) higher uncertainties are reported [42–43,60].

2.7.2 The effect of contaminated water on the dew-point temperature generation

The contamination of water in the saturator leads to the dew-point temperature drop of air exiting dew-point generator. Since the relationship between contamination of water and the dew-point temperature drop is weak highly approximative methods have been used to estimate the uncertainty due to the contamination of water in the saturator unit [34–35]. Usually the amount of contamination is calculated by measured conductivity of water in the saturator unit. Usually it is also assumed that all the ions come from LiCl that is one of the most hygroscopic salts. In order to calculate the corresponding dew-point temperature drop, the Raoult's law based calculation method is used [34–35]. In a study carried out at the NMi Van Swinden Laboratory, the composition of the water taken out of the saturator unit was analyzed with an ICP mass spectrometer giving more accurate information of the trace elements in the water [36]. According to the scarce literature about the contamination effect 1 mK represents the state of the art in the uncertainty estimation for the contamination in the dew-point generators [34–36,38,45]. Some authors have claimed that the effect is even smaller [50–51].

Recently published results of an extensive comparison of dew-point calibration systems in 22 countries show that overall uncertainties below 0.02 °C (at the 95 % confidence level) have been reached [15,61]. This suggests that the effect of water contamination may become increasingly important as the other uncertainty contributions become smaller.

2.7.3 The effect of moisture sorption and back-diffusion in trace moisture region

It is necessary for semiconductor industry to generate very dry gases [4,62,63]. It has been reported that at very low humidity values (trace moisture) the highest contribution of uncertainty comes from moisture adsorption/desorption

due to the inner surfaces of the tubing [4,64]. It is highly recommended to use internally polished stainless steel tubes while connecting humidity generators with hygrometers under calibration in the trace moisture region. The use of copper pipes is also possible if the tubing dry-down time is not paramount [64].

Another mechanism that increases uncertainty in the trace moisture region is water-vapour back-diffusion through leaks [4] or against the dry gas flow. In the latter case water-vapour will diffuse into the tubing against bulk flow of dry gas due to higher water-vapour concentration values outside the tubing than inside the tubing. In a study it has been assumed that the velocity profile of the pure gas flow is fully developed (parabolic) and the impurities diffuse into the tubing against gas flow and along the surface of the tubing due to surface concentration gradients of impurities [62]. The solution of the back-diffusion and surface diffusion equations has made it possible to calculate the minimum flow-rate to stop back-diffusion depending on the geometry of the tube and pressure inside the tubing [62].

2.8 Uncertainty sources of the secondary standard of air humidity

In many countries, national standards laboratories use secondary standards of air humidity as a routine calibration method. These are usually based on optical CMHs that serve as very stable dew-point temperature standards. In dew-point temperature calibrations sample air from a dew-point generator flows through a parallel connection of the reference CMH and calibrated dew-point hygrometer [10].

In relative humidity calibrations, the reference CMH is used together with a climatic chamber [10]. This method is also used for calibrations of dew-point hygrometers without a measurement cell. The main uncertainty components (listed in Table 1) are related to dew-point temperature or relative humidity control in the climatic chamber, uncertainty sources due to reference instruments and uncertainty sources due to the device under calibration (DUC) [65].

Table 1 Main uncertainty sources for calibrating relative humidity sensors in climatic chambers

Group	Uncertainty source	Influenced input quantity
Air humidity control		
	Spatial inhomogeneity	T, T_d or h
	Instability	T, T_d
	Radiation effect	T
	Pressure difference between the reference standard and DUC	T_d
Reference standard		
	Calibration uncertainty	T, T_d
	Curve fit	T, T_d
	Resolution of the measuring instruments	T, T_d
	Repeatability	T, T_d
	Long-term drift	T, T_d
	Self-heating	T
	Hysteresis	T, T_d
	Uncertainty of formulae	E_w, f
DUC		
	Instability of the readings	h or T_d
	Resolution	h or T_d
	Hysteresis	h or T_d

It is recommended to separate a calibration volume from the rest of the interior of a climatic chamber and study its uncertainty sources thoroughly. The temperature and relative humidity homogeneity in the calibration volume of the climatic chamber is recommended to be measured with at least 9 temperature and relative humidity probes [66–69]. One of the 9 probes is set in the middle of the calibration volume and the other 8 probes are recommended to be put into the 8 corners of the volume. The uncertainty of temperature or relative humidity homogeneity is calculated by the maximum difference between the reading of the probe in the middle of the calibration volume and the readings of the probes in the corners of the calibration volume [66]. If it can be assumed that the dew-point temperature homogeneity in the climatic chamber is very good the relative humidity homogeneity can also be calculated from the spatial homogeneity of air temperature inside the climatic chamber [69].

If the air temperature in the climatic chamber differs from the ambient temperature then the inner walls of the chamber are probably not in thermal

equilibrium with air inside the climatic chamber. Furthermore, if the emissivity of the thermometer is high, it is more susceptible to the mean radiation temperature of the inner walls and this may cause significant differences between the thermometer readings and the corresponding air temperature [66,70]. Several ways have been proposed to measure this effect. Firstly, the readings of high emissivity and low emissivity thermometers can be compared to each other. The second possibility is to put the thermometer inside a ventilated radiation shield and to compare its readings to the case if temperature is measured without the shield. It is also possible to measure the inner wall temperature of the chamber and air temperature with low emissivity thermometer. After that the maximum radiation effect can be estimated [66].

Platinum resistance thermometers are susceptible to self-heating due to the electrical current that is forced through the Pt wire for measuring its resistance as well as the thermal properties of the probe and air in contact with it. In addition, the hysteresis of industrial PRT-s due to strain of the platinum wire or film in contact with the supporting material may be significant [71]. The typical values of the hysteresis of industrial PRT-s are between 0.002 % to 0.2 % of the maximum temperature difference being measured [72].

The hysteresis of relative humidity sensors is caused by the different moisture adsorption and desorption rates in the sensors [73]. It is recommended to carry out calibration both in increasing and decreasing orders of relative humidity values in order to estimate the uncertainty due to hysteresis.

3 MODELING AND EXPERIMENTAL

3.1 Set-up of Estonian air humidity reference standard

Testing Centre, University of Tartu (TCUT) maintains, preserves and develops the Estonian reference standard for air humidity that is a secondary standard based on a Michell S4000 chilled mirror dew-point hygrometer. In order to be able to calibrate relative humidity hygrometers the sensor unit of the dew-point hygrometer as well as an industrial PRT for measuring air temperature are kept in a climatic chamber. The secondary standard setup is primarily used for realizing a relative humidity scale although it is possible to calibrate dew-point hygrometers as well.

The calibration of hygrometers is carried out in a smaller calibration volume within the climatic chamber. The calibration volume is separated from the rest of the climatic chamber by a hollow stainless steel cylinder that reflects radiated heat well. So the interior of the cylinder is assumed to achieve air temperature of the climatic chamber. The air temperature in the calibration volume is measured by a Michell industrial PRT that is calibrated against two Fluke PRTs that serve as reference thermometers. Traceability of the measured air temperature is obtained from the Estonian national temperature standard. The air temperature inhomogeneity within the calibration volume is measured by six copper-constantan differential thermocouples. The thermal voltages are measured by a digital multimeter coupled with a scanner for changing channels. The environmental conditions are measured with Ahlborn capacitive hygrometers and a pressure sensor. Air is sucked through the CMH using a pump outside the climatic chamber in order not to affect the temperature homogeneity inside the climatic chamber. Air pressure is measured within the calibration volume as well as just after the CMH in order to calculate the dew-point temperature correction due to the pressure drop in the sampling line. The condensation layer on the mirror of the reference dew-point hygrometer is observed using a microscope that is put through a port of the climatic chamber. It is necessary to distinguish between supercooled water droplets and ice crystals on the mirror, because the saturated water-vapour pressure above ice is lower than the saturated water-vapour pressure above supercooled water. The set-up of Estonian air humidity reference standard was supported by EU via Phare 2002 Project “Development of Conformity Assessment Infrastructure in the Field of Metrology” [2]. The set-up is more thoroughly described in [74].

In addition to the devices that belong to the secondary standard setup of air humidity a simple dew-point generator to work in the limited dew-point temperature range from 14 °C to 19 °C has been constructed. The main reason for constructing the simple dew-point generator is to monitor the long-term stability of the CMH between the calibrations at the foreign NMIs. The traceability chain of relative humidity measurements of TCUT is presented on Figure 4 below.

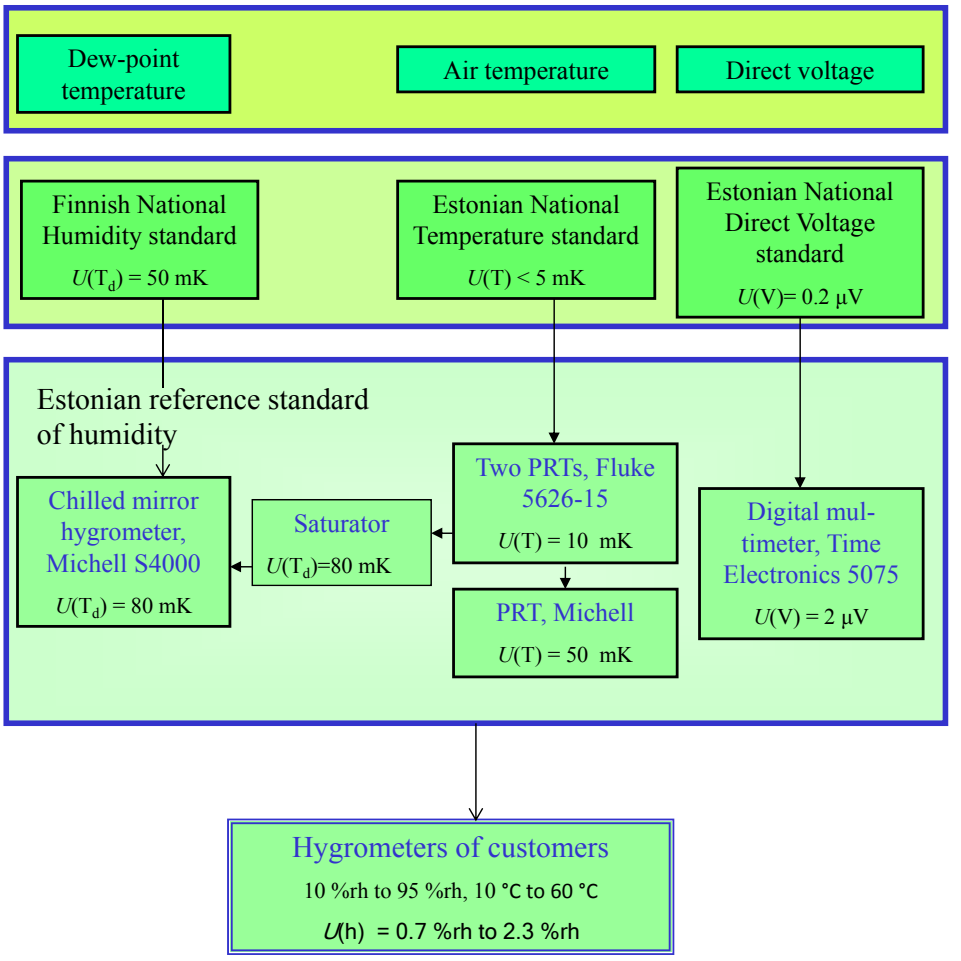

Figure 4 Traceability of relative humidity measurements. *U* is expanded uncertainty using coverage factor *k*=2

3.2 Uncertainty estimation for the reference values of relative humidity using the secondary standard

3.2.1 Mathematical model for the relative humidity reference value

The reference value of relative humidity h_{ref} is calculated according to equation (2.4). The values of enhancement factor at different temperatures and pressures applicable to the secondary standard of air humidity are presented on Figure 5.

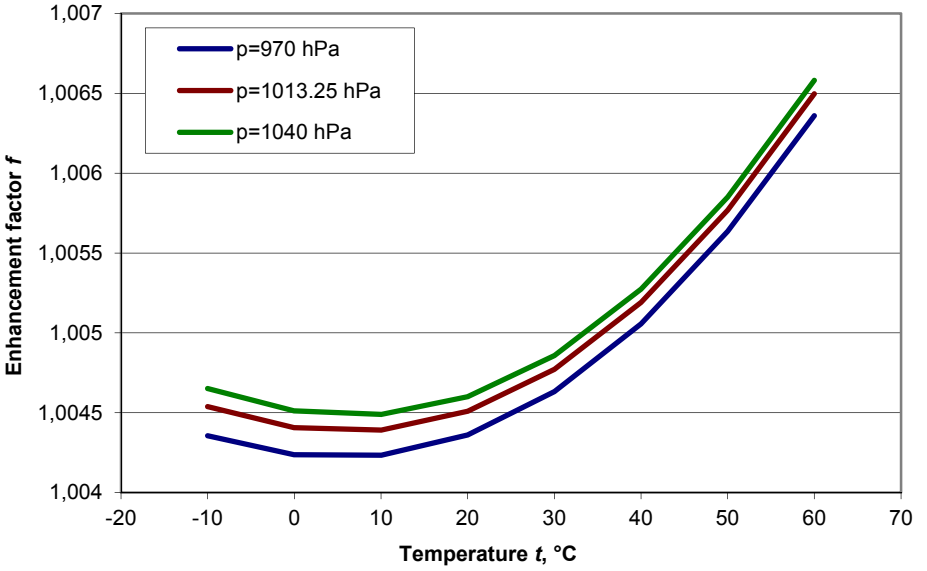

Figure 5. Enhancement factor temperature dependence at different air pressures [75]

The relative difference of the enhancement factors of air at temperatures 10 °C and 60 °C at ambient pressure 1013.25 hPa is 0.21%. For most of the practical cases the relative difference between the enhancement factors is even smaller. For this reason the enhancement factors are omitted in the relative humidity reference value formula.

The saturation water-vapour pressures with respect to water and ice at temperature T (and dew-point temperature T_d) can be calculated according to the Sonntag formula [75]:

$$E_w(T) = A_0 \cdot \exp\left[\frac{A}{T} + B + C \cdot T + D \cdot T^2 + E \cdot \ln(T)\right] \cdot \delta E_w(T), \qquad (3.1)$$

where A_0, A, B, C, D and E are the Sonntag coefficients that are presented in Table 2 below and $\delta E_w(T)$ is the relative correction of the Sonntag formula. Its value is estimated to be one and the standard deviation is 0.00005 for dew-point temperatures higher than 0 °C. For dew-point temperatures lower than 0 °C the standard deviation is 0.003 and for frost-point temperature the corresponding standard deviation is 0.005 [75].

Table 2 Sonntag coefficients for calculating saturation water-vapour pressures with respect to water and ice

Reference phase	A_0/ hPa	A/K	B	C/K^{-1}	D/K^{-2}	E
water	1	–6096.9385	16.635794	$-2.711193\cdot10^{-2}$	$1.673952\cdot10^{-5}$	2.433502
ice	1	–6024.5282	24.7219	$1.0613868\cdot10^{-2}$	$-1.3198825\cdot10^{-5}$	–0.49382577

The reference values of dew-point temperature and air temperature are calculated by the following formulae and the corresponding input quantities are explained in Table 3 below:

$$T_d = \bar{T}_d + \Delta T_{d,corr} + \delta T_{d,approx} + \Delta T_{d,p} + \delta T_{d,\mathrm{hom}} + \delta T_{d,drift} + \delta T_{d,res}, \quad (3.2)$$

$$T = \bar{T} + \Delta T_{corr} + \Delta T_{selfh} + \delta T_{approx} + \delta T_{\mathrm{hom}} + \delta T_{drift} + \delta T_{res} + \delta T_{rad}, \quad (3.3)$$

Table 3. Input quantities for dew-point temperature T_d and air temperature T reference values

Input quantity	Description
$\bar{T}_d$, $\bar{T}$	average value of dew-point temperature and air temperature readings
$\Delta T_{d,corr}$, ΔT_{corr}	calibration correction of the CMH and the thermometer
$\delta T_{d,approx}$, δT_{approx}	curve fit correction
$\Delta T_{d,p}$	pressure drop correction of dew-point temperature
$\delta T_{d,\mathrm{hom}}$, δT_{hom}	dew-point temperature and air temperature inhomogeneity correction in the calibration volume
$\delta T_{d,drift}$, δT_{drift}	long-term drift of the CMH and the thermometer
$\delta T_{d,res}$, δT_{res}	resolution correction of the CMH and the thermometer
ΔT_{selfh}	self-heating correction of air thermometer
δT_{rad}	air temperature correction due to radiation effects

3.2.2 Estimation of standard uncertainty components for air temperature and dew-point temperature

The estimation of uncertainty components is presented in details in [74]. The uncertainty component estimations have also been published in [**I**]. This section is dedicated to study the uncertainty sources that were not dealt with in [74] or were not handled in depth.

Since the air pressure in the calibration volume exceeds air pressure at the mirror of the hygrometer, it is necessary to use the dew-point temperature correction due to the pressure difference. In our case, it is possible to use the following formula [76] due to the small (about 200 Pa) pressure difference:

$$\Delta T_d = \left(\frac{\partial E_w}{\partial T_d} \right)^{-1} \cdot \Delta E_w = \frac{\frac{p_2}{p_1} - 1}{\frac{-A}{T_d^{\,2}} + C + 2 \cdot D \cdot T_d + \frac{E}{T}}, \tag{3.4}$$

where p_1 and p_2 are the air pressures on the mirror of the hygrometer and in the calibration volume, respectively, and A, C, D and E are the Sonntag coefficients (Table 2). The corresponding uncertainty can be calculated by the following formula:

$$u(\Delta T_d) = \Delta T_d \cdot \frac{u(p_1)}{p_2 - p_1}, \tag{3.5}$$

where $u(p_1)$ is the uncertainty of measuring air pressure at the mirror of the hygrometer.

The correction of self-heating of the air thermometer (industrial PRT) was determined by driving different currents through it and measuring the corresponding resistances. The currents used were in the range of 0.1 mA to 2.5 mA. The voltage just across the sensor and the current through the sensor were measured with two Time Electronics 5075 digital multimeters. So the sensor resistance was calculated as a function of current through the sensor. The difference between the resistances at zero current and the operating current (about 1.5 mA) was calculated by extrapolating the resistance function towards zero current. The self-heating correction is proportional to the measured difference in resistance. The PRT was located in the climatic chamber and one additional temperature probe was used to monitor the air temperature close to the PRT during the experiment. The self-heating correction of the industrial PRT was estimated to be –0.05 K. The error limits of the self-heating correction were estimated to be ±0.03 K by analyzing the relation between sensor resistance and current through the sensor.

In order to estimate the radiation effect due to differences between inner wall temperature of the climatic chamber and air temperature inside the chamber, a small diameter hollow metal shield was used. During the first stage of the experiment the readings of the reference thermometer inside the shield were compared to the readings of an additional thermometer close to the reference air thermometer but outside the shield. In the second stage of the experiment both thermometers were kept outside the shield. The measurements were performed at –10 °C and +80 °C. At –10 °C the air thermometer inside the small metal shield showed about 0.07 K lower value than the same thermometer outside the shield. At 80 °C the air thermometer inside the metal shield showed about 0.05 K higher value than the same thermometer outside the shield. Since another radiation shield (although bigger and opened in both end surfaces of the hollow cylinder) is used during calibration of hygrometers the correction due to the radiation effects is not applied. The potential correction is included in the uncertainty of radiation effects.

The combined standard uncertainty and expanded uncertainty for the reference value of air humidity were calculated by equations (2.6) and (2.8) using GUM Workbench 2.3 that is a special software for uncertainty estimation. Monte Carlo simulations were carried out by a special software for that purpose called MonteDist. The number of Monte Carlo trials was chosen 1 000 000. The MonteDist software was validated before use by different functions and PDF-s [**I**] for which it was possible to calculate the expanded uncertainties by traditional GUM method without having to make assumptions about the PDF-s of these functions.

3.3 The study of contaminated water on the dew-point temperature generation

3.3.1 Experimental set-up for studying the effect of contaminated water in a saturator

In order to obtain well controlled contamination a system based on intentionally prepared salt solutions was set up. The dew-point temperature drops due to low concentrations of LiCl or NaCl in water were measured directly with respect to pure water in the saturator unit of the simplified humidity generator. The direct measurement results were compared to the results of different calculation methods. The experimental set-up is presented in Figure 6 below.

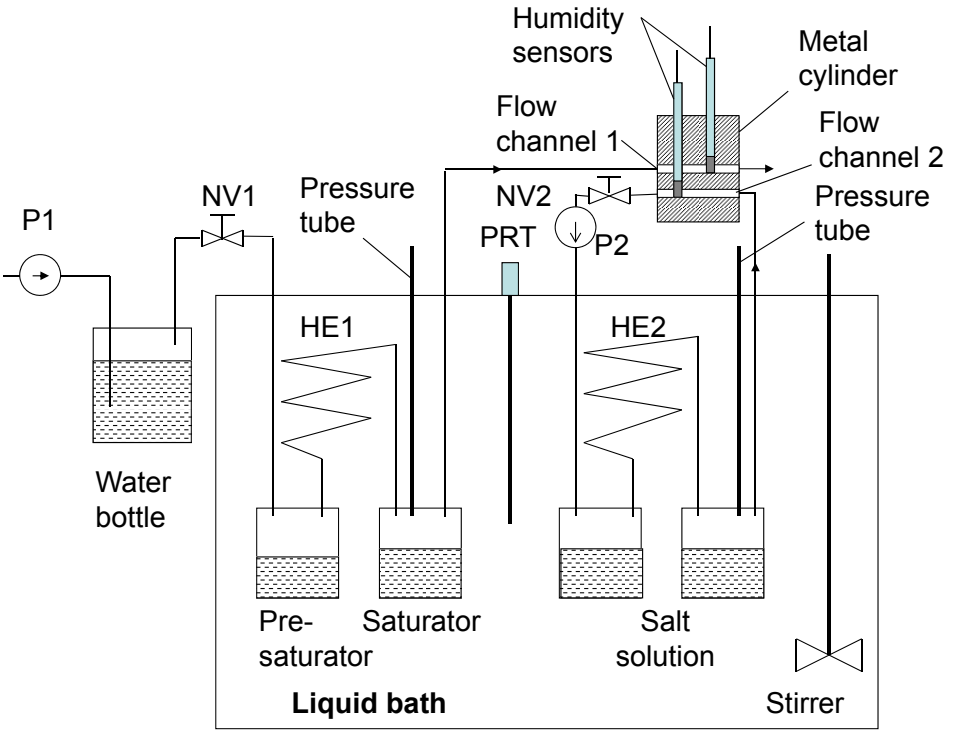

Figure 6 Experimental setup for measuring the dew-point temperature effect of well controlled water contamination. P1 and P2 – air pumps, HE1 and HE2 – heat exchangers, PRT – platinum resistance thermometer, NV1 and NV2 – needle valves

The air flows above salt solution and high purity water were totally separated. The air flow through the pre-saturator and the saturator was open and the air flow through the salt solution vessels followed a closed loop. All the four vessels had been made of stainless steel. The heat exchangers between the pre-saturator and the saturator as well as between the two salt solution vessels were made of copper pipe (both about 3 m in length). The four vessels as well as the heat exchangers were immersed in a thermally insulated temperature controlled liquid bath. The temperature inside the bath was controlled by an external thermostat. The temperature of the liquid bath was measured with a calibrated PRT. The water in the bath was constantly stirred. The saturator generated moist air in the dew-point temperature range of 14 °C to 19 °C. Laboratory air was bubbled through a water bottle in order to feed the pre-saturator and the following heat exchanger and saturator with more moist air than that of leaving the saturator. In such a case the dew-point temperature of air leaving the saturator was close to the temperature of the water in the bath because in addition to the pre-saturator much of the condensation took place in the heat exchanger as well. The copper pipes coming out of the cover of the liquid bath were slightly electrically heated to prevent the final condensation from taking

place just below the cover due to evaporative cooling of the water. It was possible to measure air pressure as well as temperature in the saturator vessel and in the second salt solution vessel. Two pumps were used to move air through the two branches of the set-up. Both air flows went through the sensor block that is a metal cylinder with two flow channels in it. The two Ahlborn FHA646-E1C capacitive humidity sensors were put into the flow channels through ports. The air pressure in the flow channels of the sensor block was slightly higher than ambient pressure. The air temperature in the laboratory was in the range of (21 ± 2) °C during the measurements.

The readings were recorded by a personal computer in every minute using the Ahlborn data acquisition program. The hygrometers were swapped in the flow channels to overcome the systematic errors related to these probes. After stabilization time of at least two hours the readings of the hygrometers were once again recorded to the computer during one hour of measurement time.
The conductivities of the salt solutions were measured before and after the dew-point temperature drop measurements using the WTW conductivity meter with TetraCon 325 conductivity cell.

3.3.2. Performance of the set-up

Before starting the measurements with salt solutions the performance of the experimental set-up was studied. For this purpose the dew-point temperature uncertainty components due to temperature inhomogeneity in the liquid bath, temperature instability, saturator efficiency and pressure measurement were experimentally determined.

The temperature inhomogeneity in the liquid bath was measured by two Fluke 5626–15 reference PRTs and one small sized PRT that could be immersed into the saturator and the salt solution vessel while monitoring the temperature in the liquid bath by the Fluke reference PRTs. The temperature in the liquid bath was measured at different horizontal and vertical locations.

The temperature instability in the liquid bath was measured by the hygrometer in the flow channel of the sensor block. The dew-point temperatures were calculated by the measured air temperature and relative humidity values. An example of the saturator dew-point temperature stability is presented on Figure 7 in case of stable air temperature in the laboratory.

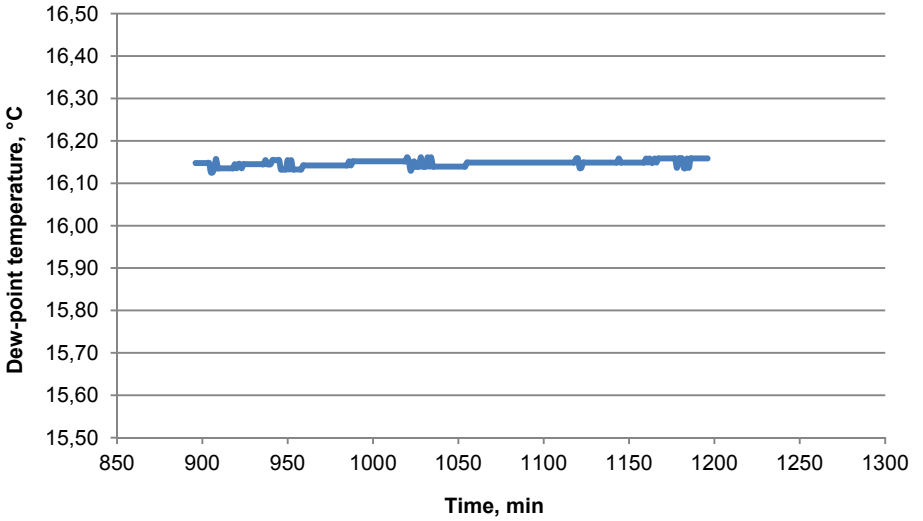

Figure 7 Stability of the dew-point temperature leaving the saturator

Saturator efficiency characterizes the agreement between the temperature of the water in the liquid bath and dew-point temperature of air leaving the saturator. Two tests were carried out to estimate the uncertainty due to inefficient performance of the saturator. Firstly, the dew-point temperature was measured by Michell S4000 chilled mirror hygrometer at liquid bath temperatures of 14 °C, 16 °C and 19 °C while the saturator was fed with air that was bubbled through the water bottle before the pre-saturator at laboratory temperature. Secondly, the dew-point temperature was measured by the chilled mirror hygrometer if the air flow-rate through the saturator was varied from 0.5 l/min to 1.5 l/min at temperature 16 °C. Since the air flow-rate through the chilled mirror hygrometer has to be 0.5 l/min, bypass was used.

Air pressure at the saturator and the second vessel for salt solutions slightly exceeds pressures in the flow channels of the sensor block. The measurement of these pressure differences also has some uncertainty.

In addition to the uncertainty sources that are related to the dew-point generator some additional uncertainty sources were taken into account. Since the air temperature drift speed in the laboratory varied from 0.1 °C/hour to 0.5 °C/hour during the one hour measurement periods and the time constant of the hygrometers' temperature sensors was measured to be about 90 s, the uncertainty of dew-point temperature due to drifting air temperature was estimated.

In another experiment all the vessels in the two branches (pure water branch and salt solution branch) were filled with high purity water. The possible differences between the results could be explained by potential leaks, different flow conditions and sorption effects of the tubing.

The outcome of the performance tests are presented as an uncertainty budget in Table 4 below.

Table 4 Uncertainty budget of the experimental set-up for measuring dew-point temperature differences between saturation with respect to contaminated and high purity water, respectively.

Uncertainty sources due to generator	**Contribution, mK**
Temperature inhomogeneity in the bath including temperature gradients in the saturator and salt solution vessels	18
Temperature instability in the bath	10
Pressure drop measurement	5
Saturator efficiency	20
Temperature measurement with PRT	20
Uncertainty sources due to measurement with capacitive hygrometers	
Resolution of the hygrometers	10
Air temperature drift in the laboratory	10
Other effects (different air flow at the two measurement locations inside the sensor block, possible leaks, sorption effects)	30
Combined standard uncertainty	**49**
Expanded uncertainty (*k*=2)	**100**

The expanded uncertainty (k=2) of dew-point temperature generation of the simplified dew-point generator is estimated to be 80 mK.

3.3.3. Measurement of the amount of natural contamination

The natural contamination is named to be the amount of ions and organic compounds that come only from the inner walls of the saturator vessels and additionally by sampling. The natural contamination of water samples in vessels of different materials was determined in closed vessels as well as in ventilated vessels. In the first stage of the experiment stainless steel, copper, glass and plastic (polypropylene) vessels were filled with ultra-high purity water (ρ = 18.2 MΩ cm, TOC < 4 ppb) after being cleaned with methanol, high purity water and ultra-high purity water. The ultra-high purity water was produced by Milli-Q Advantage A10 water purification system. The water samples were kept in the vessels for about 13 months. After that the total organic carbon (TOC) values and conductivities were measured with Millipore A10 TOC monitor and WTW conductivity meter with TetraCon 325 conductivity cell. The dilution method was used for the measurement of TOC values because the TOC monitor consumed more water than it was in the vessels. In addition to conductivity and

TOC value measurements the content of different metal ions was determined in the stainless steel and copper vessels by the company AS Tallinna Vesi laborid using the Agilent 7500a ICP-MS trace metals analyzer.

In the second stage of the experiment the water samples were kept in the 4 closed vessels as well as in the 4 ventilated vessels at the same time for about 70 days. This stage of the experiment showed how much additional contamination came from sampling. The air from the central compressed air system (filter element XP with filtration efficiency 99.99999%) of UT Institute of Chemistry was blown above the samples of water in the vessels. A water bottle was placed between the compressed air line and the vessels and the air was bubbled through the water in order to saturate it for reducing the drying of the vessels. The water bottle was filled several times during the experiment. For practical reasons the four vessels were connected in parallel to each other using copper pipes (in order to get a conservative, i.e. not optimistic, estimate of the contamination effect). All the four branches were prepared of almost the same length. After about two months the similar set of measurements and analyses were carried out in order to estimate the contamination of the water samples.

3.3.4 Calculation of the effect of natural contamination on the dew-point temperature generation

The calculation of dew-point temperature drops due to contamination in the water samples is based on measuring conductivities in the four different material vessels and making some assumptions about the composition of the water samples. For stainless steel and copper vessels the concentration of different metal ions had been measured by ICP-MS device. It was assumed that HCO_3^- was the only anion in the water samples. The concentration of HCO_3^- ions can be calculated by the concentration of most abundant metal ions assuming that the condition of electroneutrality of the water samples is fulfilled. For glass and plastic vessels it was assumed that all the cations were Na^+ ions and all the anions were HCO_3^- ions. The conductivity of the water samples σ_1 can be calculated by the molar concentration of most abundant metal ions c_i and the molar concentration of HCO_3^- ion c_a by the following formula:

$$\sigma_1 = \sum_i \lambda_{0,i} \cdot c_i + \lambda_{0,a} \cdot c_a \,, \tag{3.6}$$

where $\lambda_{0,i}$ and $\lambda_{0,a}$ are the limiting molar conductivities of the most abundant metal ions and the HCO_3^- ion, respectively. The molar concentration of ions in the water samples were calculated by the following formula:

$$c_2 = \frac{\sigma_2}{\sigma_1} \cdot (\sum_i c_i + c_a) \tag{3.7},$$

where σ_2 represents the directly measured conductivity of a water sample. Assuming that the water samples are very dilute the amount fraction of ions in the water samples *x* can be calculated by the following formula:

$$x = \frac{c_2}{c_w + c_2} \approx \frac{c_2}{\frac{\rho_w}{M_w} + c_2} \tag{3.8},$$

where ρ_w and M_w are the density and the molar mass of water, respectively. The water-vapour pressures above the naturally contaminated water samples e_w were calculated using the Raoult's law:

$$e_w = (1 - x) \cdot E_w , \tag{3.9}$$

where E_w is the saturated water-vapour pressure above pure water that was calculated by the Sonntag formula (3.1). The inverse of the Sonntag formula [75] was used to calculate the dew-point temperature above the naturally contaminated water samples. This dew-point temperature was compared to the initial dew-point temperature for calculating the dew-point temperature drop due to natural contamination of the water samples.

3.3.5 Different calculation methods for ionic contamination of water

Three methods were used to calculate the water-vapour pressures above salt solutions in the vessels that were set inside the liquid bath of a simplified dew-point generator. These methods are based on the Raoult's law, Conde formulae [77] and data by Fontana [78]. The usage of these methods is described in more detail in [**II**]. In addition to these three calculation methods dew-point temperature drops due to salt solutions were directly measured by two capacitive hygrometers in the sensor block (metal cylinder).

3.4 Study of leaks in the sampling line in the trace moisture region

3.4.1 Experimental set-up and description of measurements

Experiments and theoretical studies were carried out to estimate the significance of frost-point temperature error due to leaks in humidity calibration systems. Leaks in the tubing as well as in two connectors were studied experimentally at the MIKES humidity laboratory. The absolute pressure of about 1220 hPa was

maintained in the sampling line. So water molecules could only enter into the tubing via the mechanism of back-diffusion, i.e. diffusion of water molecules against the bulk outward flow of air through the hole in the tubing. In addition to the positive gauge pressure the leakage of water-vapour into the tubing depends on the leak hole geometry, water-vapour pressure difference across the tube wall and flow profile of air through the leak hole. Leaks through tiny holes intentionally drilled through tube walls were studied in this work instead of actual connectors for simplicity. In a leaking connector gas molecules are exchanged with ambient through a path with a complex and possibly unstable geometry but in a drilled hole the geometry is well defined.

For the first part of the experiment holes of different diameter (0.05 mm, 0.1 mm, 0.2 mm and 0.5 mm) were burned in the walls of internally polished stainless steel tubes using a laser based system. The wall thickness of the 6 mm outer diameter tube was 1 mm. The effect of leak flow-rate on the dew-point temperature change was measured. The experimental set-up is presented in Figure 8 below. Dry air generated by the MIKES dew/frost-point generator (MDFG), flew through a tube with a leak hole and entered the MBW 373 CMH. The tube with a leak hole was in a cell containing air saturated with respect to water at ambient temperature. The dew-point temperatures of air leaving the generator were compared to the CMH readings. The PTB220 digital barometer was used for measuring pressure difference between the dew-point generator and the CMH in order to calculate the dew-point temperature drop due to the pressure loss in the sampling line. The leak flow-rate was controlled by a mass flow controller between the cell and ambient air. The mass flow controller had been calibrated at the MIKES flow laboratory. Liquid water on the bottom of the cell and a wet sleeve wrapped around the tube with a leak hole ensured that the air at the leak hole would be saturated with respect to water. The ambient conditions of the laboratory were measured by a Vaisala capacitive hygrometer.

In reality the leakage of air through the connectors is much more probable than leakage through possible holes in the wall of the tubing. Therefore in the second part of the experiment the back-diffusion of water-vapour through leaking connectors was studied. The connectors were exposed to ambient air. The Swagelok and VCR connectors between the MDFG and the CMH were loosened for this purpose. The air flow-rate through the chilled mirror hygrometer was kept constant. The mass flow-rate of leaking air was measured as a difference of the two flow-meter readings that were connected before the MDFG and after the chilled mirror hygrometer.

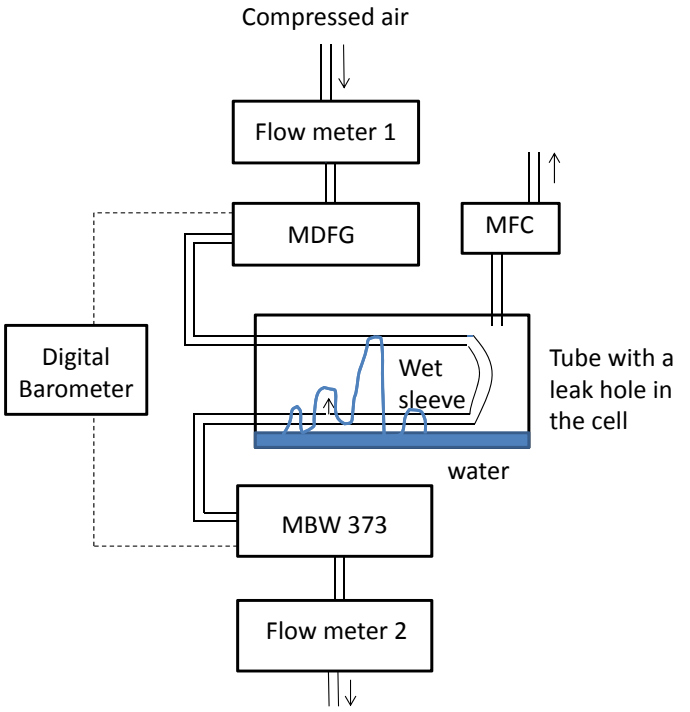

Figure 8. Experimental set-up for measuring the frost-point temperature change due to the leak hole in the tube, MDFG – MIKES dew/frost-point generator, MFC – mass flow controller, MBW 373 – CMH

3.4.2 Calculation of the critical flow-rate of air through the leak hole

According to the Fick's first law the diffusion flow-rate of water-vapour into the tubing depends on the water-vapour concentration across the hole inside the wall of the tubing, the geometry of the hole and binary diffusion coefficient of water-vapour molecules in air if there is no air movement through the leak hole. If the pressure inside the tubing is higher than outside air moves out of the tubing. At low air flow-rates it is still possible for water-vapour molecules to diffuse inside the tubing against air flow. If the air flow-rate through the leak hole becomes higher less water-vapour molecules will diffuse against the moving air into the tubing. At a certain flow-rate of air out of the leak hole it is possible that no detectable amount of water-vapour molecules diffuse into the tubing. This flow-rate is named the critical flow-rate.

The critical flow-rate of dry air to stop water molecules from diffusing into the flowing dry air is derived. It has been assumed that the flow-profile of the dry air leaking out of the tube is flat. The problem is treated one-dimensionally.

Figure 9 illustrates the escape of water molecules into the tubing via the mechanism of back-diffusion.

In a binary mixture (dry air and water-vapour) the mass flux $[n''_w] = (\mathrm{kg\ m^{-2}\ s^{-1}})$ of water-vapour in a fixed coordinate system n''_w can be calculated according to the following formula [79]:

$$n''_w = -D_{aw} \cdot \rho \cdot \frac{\partial m_w}{\partial y} + m_w (n''_a + n''_w) \qquad (3.10),$$

where the first term describes the diffusive flux of water molecules with respect to the mass-average flux of water-vapour and dry air mixture and the second term characterizes the flux of water molecules moving at mass-average velocity with respect to the fixed coordinate system. In equation (3.10) ρ is the density of air, D_{aw} is the binary diffusion coefficient, m_w is the mass fraction of water-vapour in air, n''_a is the mass flux of dry air through the leak hole in fixed coordinate system and *y* shows the direction of the movement of dry air out of the leak hole.

By setting the mass flux of water molecules n''_w zero in equation (3.10) yields the following differential equation:

$$\int_0^L n''_a dy = \rho \cdot D_{aw} \int_{m_{w0}}^{m_{wL}} \frac{dm_w}{m_w} \qquad (3.11),$$

where m_{w0} is the mass fraction of water-vapour at the inner surface of the tube and m_{wL} is the mass fraction of water-vapour at the outer surface of the tube with wall thickness *L*.

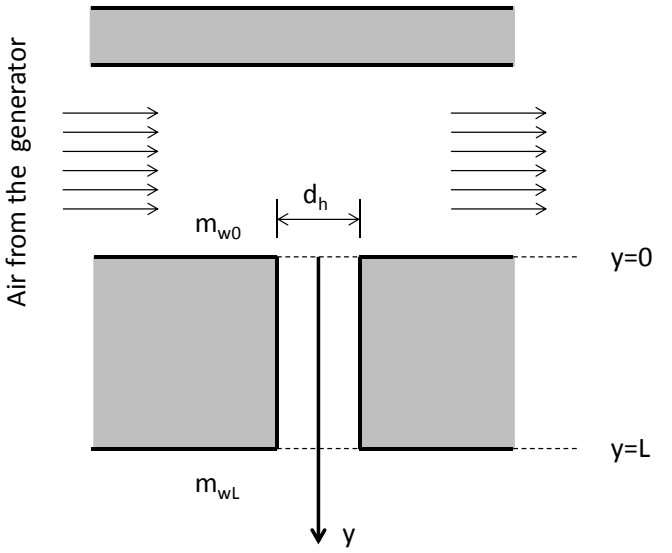

Figure 9. Water-vapour leakage into the tubing via the mechanism of back-diffusion

By solving the equation for the critical dry air mass flux n''_a and expressing the result as critical volume flow-rate $[Q_{cr}]$ = (m^3 s^{-1}), the following equation is obtained:

$$Q_{cr} = \frac{\pi \cdot D_{aw} \cdot d_h^{\,2}}{4 \cdot L} \cdot \ln\left(\frac{m_{wL}}{m_{w0}}\right) \qquad (3.12),$$

where d_h is the leak hole diameter.

It has been assumed that the mass fraction of water-vapour at the outer surface of the tube equals to the mass fraction of water-vapour in the cell and the mass fraction of water-vapour at the inner surface of the tube equals to the mass fraction of water-vapour inside the tube:

$$m_{wL} = \frac{E_w(T_2) \cdot f(T_2, p_2) \cdot M_w}{R \cdot T_2 \cdot \rho} \qquad (3.13)$$

and

$$m_{w0} = \frac{E_w(T_1) \cdot f(T_1, p_1) \cdot M_w \cdot \dfrac{p_2}{p_1}}{R \cdot T_2 \cdot \rho} \qquad (3.14).$$

In equations (3.13) and (3.14) M_w is the molar mass of water, R is the molar gas constant, ρ is the density of air, T_1 and T_2 are the absolute temperatures in the saturator unit of the MDFG and in the cell, respectively, p_1 and p_2 are the air pressures in the saturator unit of the MDFG and in the cell, respectively. The saturated water-vapour pressures at temperature T are calculated using the Sonntag formula [75]. In equations (3.13) and (3.14) $f(T,p)$ is the enhancement factor of moist air [75].

4 RESULTS AND DISCUSSION

4.1 Uncertainty estimation for the relative humidity reference value using the secondary standard of humidity

4.1.1 Comparison of uncertainties using three approaches

It is important to estimate the uncertainty of a measurand using different approaches in order to reveal possible calculation errors and the possible influence of the different assumptions made in different approaches. For this reason the reference values of relative humidity, standard deviations and corresponding expanded uncertainties were calculated using the traditional GUM method, the MCM and GUM modified by Bayesian approach. The results are presented in Table 5.

The uncertainty budgets for medium and high relative humidity cases are presented in Appendix 1 in tables A1 and A2. These uncertainty budgets contain data about values, PDFs and estimated standard uncertainties for all the input quantities as well as their contributions to the corresponding combined standard uncertainties.

The PDFs obtained by the Monte Carlo method are compared with normal distributions and Student's t-distributions at medium and high relative humidity values in figures 10 and 11, respectively.

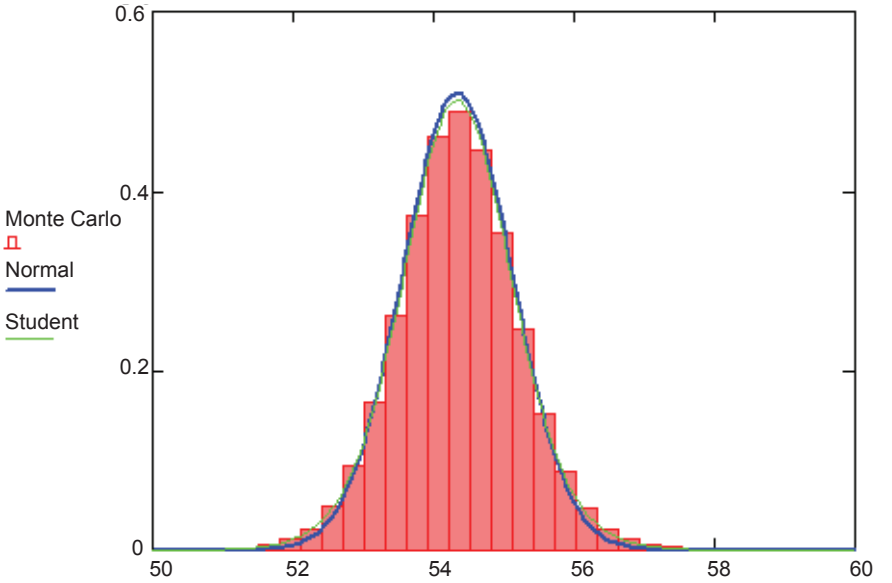

Figure 10. The comparison between the PDFs obtained by the Monte Carlo Method, the Normal distribution and the Student's t-distribution with 14 degrees of freedom in the case of medium relative humidity values (on the horizontal axis)

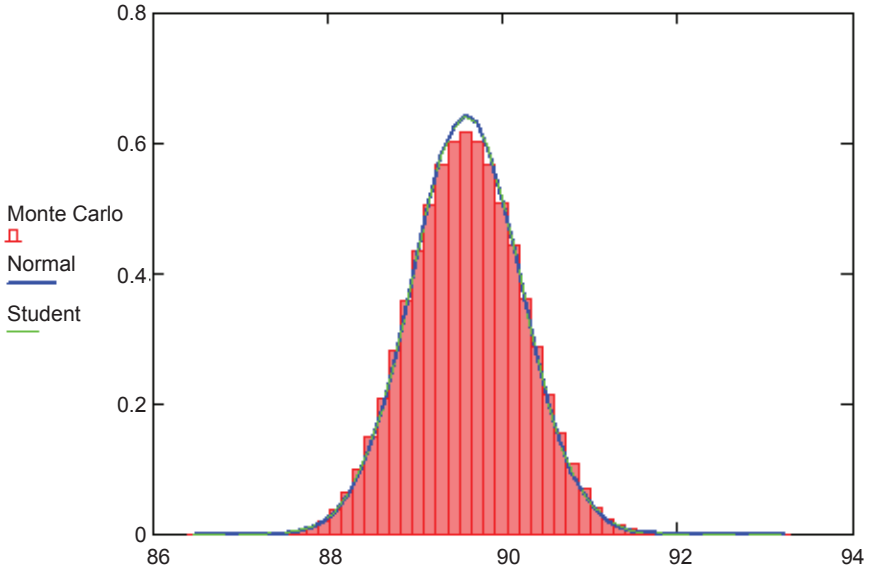

Figure 11. The comparison between the PDFs obtained by the MCM, the Normal distribution and the Student's t-distribution with 240 degrees of freedom in the case of high relative humidity values (on the horizontal axis)

Table 5 Comparison of the measurement results between the traditional GUM method, MCM and the GUM modified by Bayesian approach in the case of medium and high relative humidity reference values

	Medium relative humidity			High relative humidity		
	GUM method	MCM	Bayesian method	GUM method	MCM	Bayesian method
Mean value	54.34 %rh	54.35 %rh	54.34 %rh	89.58%rh	89.58 %rh	89.58 %rh
Standard deviation	0.783 %rh	0.869 %rh	0.868 %rh	0.619 %rh	0.638 %rh	0.639 %rh
Effective degrees of freedom	14	–	–	240	–	–
Student's t-coefficient	2.20	–	2.00	2.00	–	2.00
Expanded uncertainty	1.72%rh	1.76 %rh	1.74 %rh	1.24 %rh	1.27 %rh	1.28 %rh

The agreement between the three methods is good. The traditional GUM method using the Welch- Satterthwaite formula for calculating the number of effective degrees of freedom for the measurand underestimates the expanded uncertainty by as little as 0.04 %rh percent compared to the MCM. The

agreement between the Monte Carlo method and the GUM modified by Bayesian approach is even better. These two approaches estimate the standard uncertainty of the Student's t-distribution in a similar way according to equation (2.10). It is possible to use all these methods to estimate uncertainty for the two relative humidity cases. However, at medium relative humidity values it is necessary to take into account the coverage factor of 2.20 due to the 14 effective degrees of freedom of the measurand if traditional GUM method is being used. For high relative humidity values the number of effective degrees of freedom is estimated to be 240 and the corresponding coverage factor is k=2.00.

The uncertainties of reference values at medium relative humidities are relatively large due to the dew-point temperature instability in the climatic chamber. The relative humidity correction for the hygrometer under calibration is in fact significantly smaller because the reference dew-point temperature and the relative humidity readings of the calibrated hygrometer are highly correlated if the readings are taken at almost the same time. This correlation is automatically taken into account when applying the traditional GUM method for the expanded uncertainty of the correction of device under calibration.

4.1.2 The stability of the chilled mirror hygrometer

It is useful to compare the CMH dew-point temperature readings with simplified dew-point generator liquid bath temperature readings in order to assess the temporal stability of dew-point temperature measurement. The differences between the reference chilled mirror hygrometer dew-point temperature and liquid bath temperature readings are shown on Figure 12 below. All the known corrections have been taken into account. The data have been collected during June 2012 to May 2014. It can be seen that the deviations are lower than both the chilled mirror hygrometer and the simplified dew-point generator expanded uncertainties. On an average the readings of the chilled mirror hygrometer are by about 0.03 °C lower than the liquid bath temperature of the simplified dew-point generator. The stability of the chilled mirror hygrometer dew-point temperature readings with respect to the liquid bath temperature readings is reasonably good compared to the corresponding expanded uncertainties.

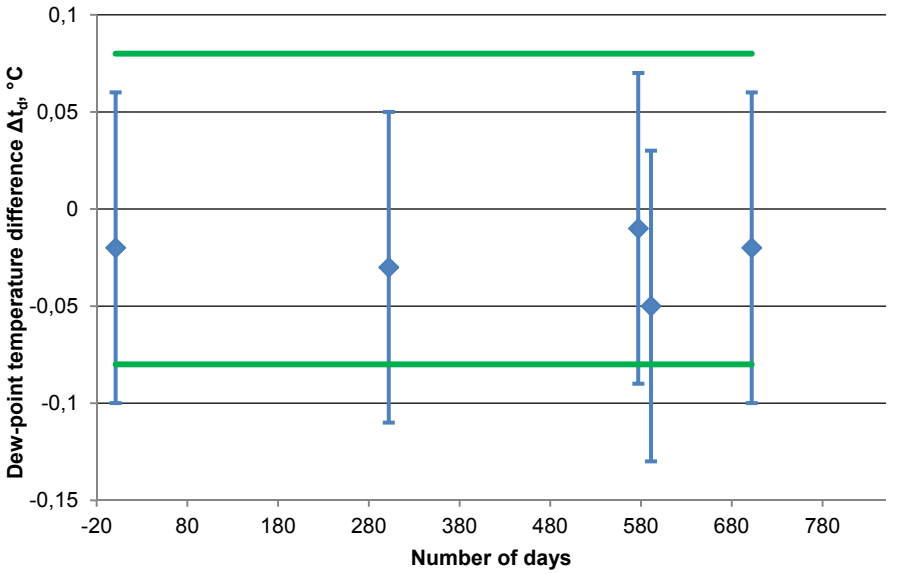

Figure 12. The difference between the dew-point temperature measured by the chilled mirror hygrometer and temperature of the liquid bath of the simplified dew-point generator (blue points). The expanded uncertainties of the chilled mirror hygrometer are presented by blue error bars and the expanded uncertainties of the liquid bath temperature measurements are marked by green lines.

4.1.3 Interlaboratory comparisons

TCUT has taken part in three international interlaboratory comparisons in the field of relative humidity and in one air temperature international inter-laboratory comparison. The results of the first bilateral interlaboratory comparison between MIKES and TCUT are presented in [74]. The other two relative humidity interlaboratory comparisons were organized by Danish Technological Institute. The name of these two interlaboratory comparisons held in 2007 and 2011 is "Calibration of a digital portable humidity and temperature instrument" and the short names are written as HUMI-02 and HUMI-03, respectively. The results of the two interlaboratory comparisons are presented in tables 6 and 7 below. The normalized errors in tables 6 to 8 are calculated using the following formula:

$$E_n = \frac{X_{TCUT} - X_{ref}}{\sqrt{U_{TCUT}^2 + U_{ref}^2}}, \tag{4.1}$$

where X_{TCUT} and X_{ref} are the relative humidity or air temperature readings of TCUT and the pilot laboratory, respectively. In equation (4.1) U_{TCUT} and U_{ref} are the corresponding expanded uncertainties at k=2 level.

Table 6. The results of TCUT at the HUMI-02 interlaboratory comparison

Temperature, °C	Relative humidity nominal value, %rh	Expanded uncertainty of the relative humidity reference value, %rh	Expanded uncertainty of relative humidity measured by TCUT, %rh	Mean deviation $h_{TCUT} - h_{ref}$, %rh	Normalized error E_n
25	10	0.63	0.7	–0.2	–0.21
25	35	1.1	0.8	–0.3	–0.22
25	50	0.94	1.0	–0.2	–0.17
25	75	1.4	1.3	–0.4	–0.24
25	90	1.1	1.5	–0.5	–0.27

Table 7. The results of TCUT at the HUMI-03 interlaboratory comparison

Temperature, °C	Relative humidity nominal value, %rh	Expanded uncertainty of the relative humidity reference value, %rh	Expanded uncertainty of relative humidity measured by TCUT, %rh	Mean deviation $h_{TCUT} - h_{ref}$, %rh	Normalized error E_n
25	10	0.32	0.9	–0.1	–0.1
25	50	0.48	1.4	–0.6	–0.4
25	95	0.69	1.8	–0.4	–0.2
45	50	0.49	1.3	–0.1	–0.1
45	95	0.69	1.7	0.0	0.0

The results in tables 6 and 7 show a good agreement between the relative humidity measurements between Danish Technological Institute and TCUT since in all the cases E_n<0.5.

TCUT has also taken part in the EURAMET Project P1061 – Comparison of air temperature calibrations. The results for the combination of high and low emissivity thermometers are presented in Table 8 [80].

Table 8. The comparison results for the combination of high emissivity and low emissivity thermometers

Nominal temperature, °C	Mean deviation $T_{TCUT} - T_{ref}$, °C	Expanded uncertainty (TCUT), °C	Normalized error E_n
–10	–0.092	0.094	–1.0
10	–0.055	0.094	–0.5
20	–0.035	0.094	–0.4
50	–0.026	0.104	–0.3
80	–0.041	0.118	–0.4

It can be seen in Table 8 that in all the cases the reference value of air temperature estimated by TCUT is lower than that estimated by MIKES. It is possible that the self-heating correction of TCUT air thermometer (–0.07 °C) was overestimated. At temperature –10 °C the uncertainty of radiation effects has probably been underestimated. It is possible that the thermal shielding is not sufficient due to the open ends of the hollow metal cylinder and the high emissivity thermometer absorbs significantly more heat from the hotter surfaces of the climatic chamber inner walls than the low emissivity reference thermometer.

In the case of thermohygrometer all the deviations from reference values were between –0.06 °C to 0.06 °C, i.e. the deviations are well within the estimated expanded uncertainties.

The air temperature best measurement capability of TCUT has been estimated as 0.2 °C for the whole accredited measurement range –10 °C to 80 °C. This is in agreement with the comparison results.

4.2 The effect of water contamination on the dew-point temperature generation

The results of the content of most abundant metal ions in the stainless steel and copper vessels are presented in Table 9 below. The last row of the table shows the minimum value for the content of all the metal ions in the water samples taking also into account the corresponding expanded uncertainties.

Table 9 The content of different metal ions[a] in the water samples kept in stainless steel and copper vessels for different periods

Metal ions	copper vessel		stainless steel vessel	
	Closed during 13 months	Air flow during 2 months	Closed during 13 months	Air flow during 2 months
	µg/l	µg/l	µg/l	µg/l
Na^+	90±10	350±35	50±6	320±32
Mg^{2+}	70±7	52±6	20±2	6±1
Ca^{2+}	320±26	370±28	40±18	20±17
Mn^{2+}	–	–	46.3±3.7	5.2±0.5
Ni^{2+}	34.5±2.1	9.0±0.5	1.0±0.1	1.0±0.1
Cu^{2+}	1158±93	1450±116	4.4±0.4	360±29
Zn^{2+}	23.7±2.6	192±21	5.8±0.7	147±16
Ba^{2+}	–	12±1	0.60±0.06	6.0±0.6
Σ	> 1550	> 2230	> 14–0	> 770

[a] Measurement uncertainties are given at $k = 2$ level

The high copper content in the ventilated stainless steel vessel can be explained by copper tubing between the water bottle that reduces the drying of the ventilated vessels and the stainless steel vessel itself.

The results of TOC measurements of the water samples kept in different material vessels for different periods are presented in Table 10 below.

Table 10. TOC values[a] of the water samples that have been kept in the vessels for different periods.

Vessel material	Closed during 13 months	Closed during 2 months	Air flow during 2 months
	TOC / ppb	TOC change / ppb	TOC change / ppb
Stainless steel	1800	240	410
Copper	1000	200	630
Glass	2000	330	420
Plastic	2500	210	560

[a] Relative expanded ($k = 2$) uncertainties are 40% based on the data by repeated measurements and taking into account the uncertainties due to the dilution method and the permissible error of the TOC monitor.

The TOC value is highest in plastic vessel and lowest in copper vessel for water samples that have been kept in the vessels for 13 months. Since the volume of the plastic vessel was around two times bigger than that of other material vessels the TOC value in the plastic vessel can be considered somewhat

underestimated. For 2 months period there is no clear dependence of the vessel materials on the TOC values of water samples. However, the TOC values in ventilated vessels are roughly two times higher than the TOC values in the closed vessels. This can be explained by the additional contamination coming from the sampling. It can also be seen in Table 10 that the TOC values of the water samples that were kept in the vessels for 13 months exceed the TOC values of water samples that were kept in the vessels for 2 months by roughly 7 times.

The calculated dew-point temperature drops due to water-samples in different material vessels are presented in Table 11. The estimated expanded uncertainties (k=2) range from 2 μK to 10 μK. According to the results presented in Table 11 the highest dew-point temperature change rate of 26 μK/month was found in the case of ventilated copper vessel. The data in Table 11 also show that the dew-point temperature change rate due to ionic contamination decreases in time. For this reason the actual dew-point temperature change during the first month might be even higher than 26 μK. In a similar study carried out by Nielsen and de Groot [36] the dew-point temperature change rate of 140 μK/week was observed that is almost by an order of magnitude higher than the dew-point temperature change rate reported in this thesis. This difference can be partly explained by probably more flat shape of the saturator vessel at NMi van Swinden Laboratory compared to the vessels used in this study. For this reason the surface to volume ratio of the saturator vessel used by Nielsen and de Groot is relatively higher and this can increase the rate of water contamination. Another reason might be the possibly higher air flow-rate through the saturator at NMi van Swinden Laboratory compared to (0.3 ± 0.1) l/min that was used in this study.

Table 11. Dew-point temperature drops (Δt_d) corresponding to the directly measured conductivities for the water samples that have been kept in the vessels for different periods.

Vessel material	**Closed during 13 months**	**Closed during 2 months**	**Air flow during 2 months**
	Δt_d/μK	Δt_d/μK	Δt_d/μK
Stainless steel	10	7	17
Copper	28	18	51
Glass	44	13	22
Plastic	14	11	14

In order to compare the effects of the inorganic and organic compounds on the water-vapour pressure it is necessary to convert the data in tables 9 and 10 to amount fractions. In order to do this it is necessary to make some assumptions what could be the organic contaminants. It is reasonable to assume that these are largely biomolecules, such as lipids, mucous compounds, proteins/peptides,

polysaccharides, etc. 1000 g/mol is taken as a crude and conservative (probably the average molar mass is in fact higher) estimate of the average molar mass. Taking 2000 ppb as an estimate of the TOC leads to amount fraction of $3.6 \cdot 10^{-8}$. A similar amount fraction estimation for the inorganic contamination at roughly 100 μmol l^{-1} (taking into account both anions and cations) leads to an amount fraction estimate of $1.8 \cdot 10^{-6}$, which is roughly 50 times higher than in the case of the organic contaminants. Therefore we can neglect the organic contaminants when the dew-point temperature drops are calculated by the Raoult's law and take into account only the ionic contamination (including the counteranions).

According to the data presented in Table 11 the highest dew-point temperature drop due to contamination is estimated not to exceed 0.07 mK in 2 months if the expanded uncertainties (k=2) and the possible effect due to organic contamination is being taken into account. This is more than an order of magnitude smaller result than the conservative estimate of 1 mK reported by several authors [34–35, 41]. The differences between the results may be due to inaccuracies in the applied measurement methods or different initial cleanness of the saturator vessels and the tubing. Also potential corrosion at welding joints and other spots in the saturators may have caused higher contamination rates.

Different methods to calculate the dew-point temperature drops due to intentionally prepared NaCl and LiCl aqueous solutions are compared to each other and to the results of direct measurements on figures 13 and 14 below. The direct measurement results agree well with different calculation methods. The Raoult method also agrees well with other calculation methods giving slightly higher dew-point temperature drop values at lower salt solution concentrations and slightly lower values at higher salt solution concentrations. This is in line with the limitations of the Raoult's law. Therefore, using Raoult's law to calculate dew-point temperature drops due to contamination in the saturators is well justified.

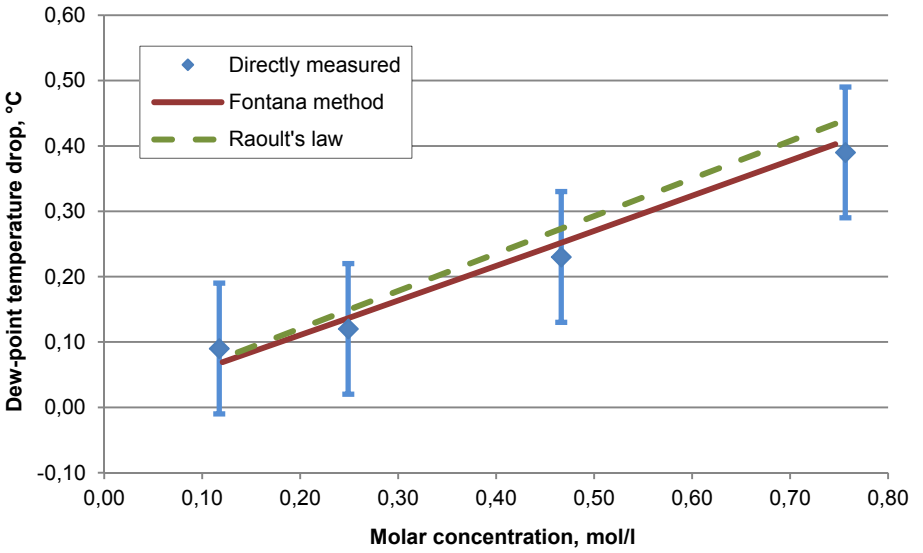

Figure 13. Comparison of the directly measured and calculated drops in dew-point temperature for NaCl aqueous solutions at T=16 °C using Fontana's data and Raoult's law

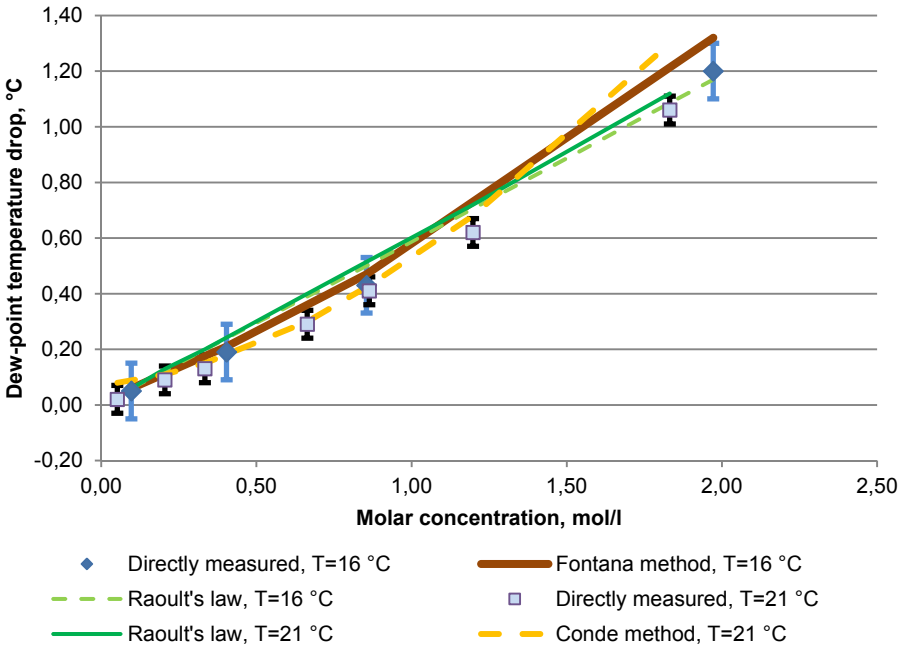

Figure 14. Comparison of the directly measured and calculated drops in dew-point temperature for LiCl aqueous solutions at 16 °C and 21 °C using Fontana's data, the Conde method and the Raoult method

4.3 The effect of leaks in a sampling line on the dew-point temperature of air

The calculated and measured critical leak flow-rates through holes in the tubing are presented on Figure 15 below. It can be seen that the agreement between the measured and calculated critical flow-rates at the frost-point temperature of –80 °C is good although the calculation method is simplified as described in section 3.4.

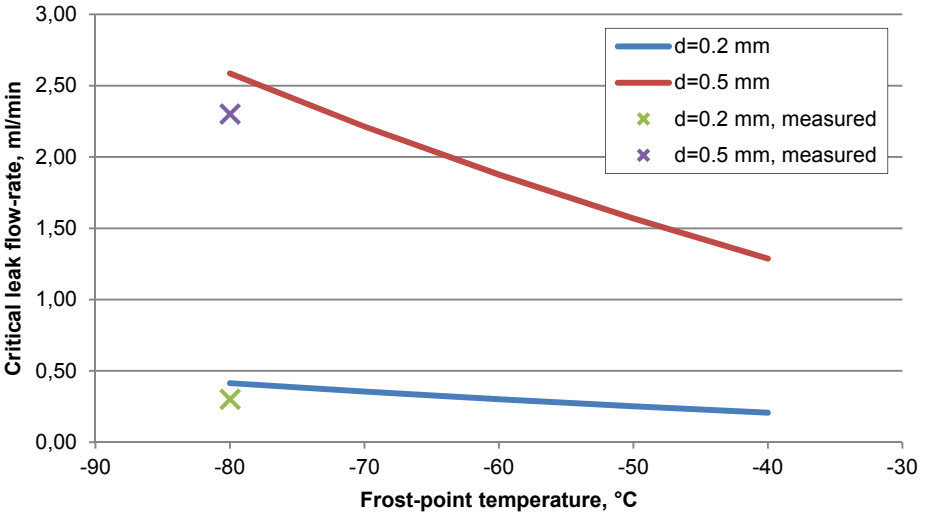

Figure 15. Critical leak flow-rates to stop back-diffusion through different diameter leak holes at different frost-point temperatures

In reality the water-vapour back-diffusion may take place in connectors. For a VCR connector the measured critical flow-rate at the frost-point temperature of –80 °C is presented in Figure 16. The leak flow-rate through the connector is varied between 20 ml/min and 550 ml/min and the critical flow-rate is found to be 100 ml/min. Experiments with Swagelok and VCR connectors showed that the latter is more sensitive to the back-diffusion effect. This can be explained by the different geometry of the connectors. The flow path through the Swagelok tube fitting is longer preventing water-vapour molecules from back-diffusing into the tubing more efficiently.

While performing practical measurements the air flow-rate through the connector depends on the pressure difference across the wall of the tubing and the geometry of the loosened connector. This is different from the leak hole experiment where the leak flow-rates of dry air through the holes were set by mass-flow controllers. It is possible that the leakage of water molecules into the tubing through a small hole even exceeds the leakage through a bigger hole

provided that other conditions are the same. It can be explained by lower air speed through the smaller leak hole.

It is of course not recommended to loosen connectors in order to achieve smaller back-diffusion of water molecules. While loosening connectors there is a very small volume where the net velocity of molecules is high. Major part of the gas volume is close to a solid surface where net velocity of molecules is low or very low. This enables water molecules to diffuse into the tubing.

The results of this study show that maintaining positive gauge pressure in the tubing effectively prevents water-vapour back-diffusion into the tubing even if the frost-point temperature of air inside the tubing is –80 °C. The smaller leaks can also potentially lead to higher diffusion of water molecules into the tubing as can be seen on Figure 16 below.

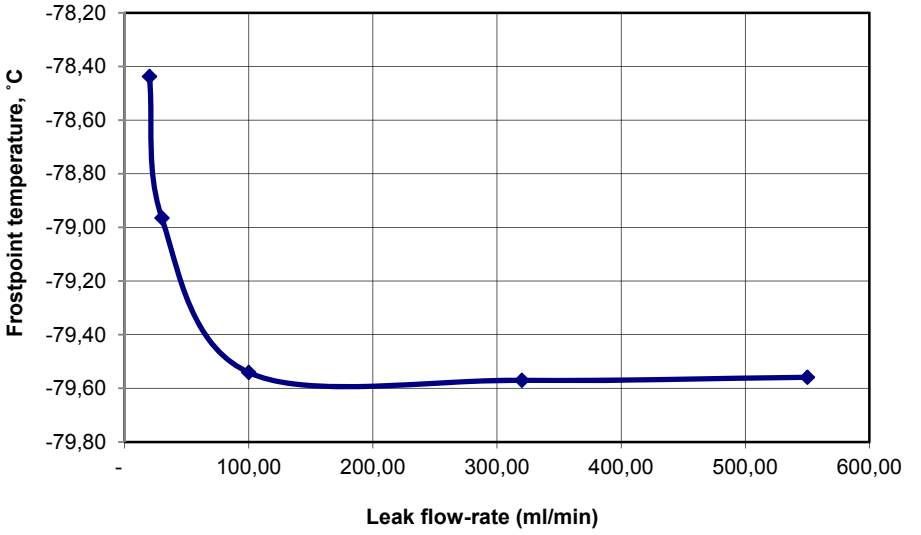

Figure 16. The effect of leak flow-rate through a VCR connector on the frost-point temperature of air in the tubing

4.4 Possible future development of Estonian reference standard of air humidity

The present simplified dew-point generator is suitable for stability checking of the chilled mirror hygrometer in a limited dew-point temperature range but does not yet meet the possible future needs. Furthermore, since the permissible errors of hygrometers tend to decrease in time it may be necessary to construct a humidity generator working in the dew-point temperature range –50 °C to 60 °C. It may be necessary to extend the dew-point temperature generation range down to –50 °C in order to be able to calibrate hygrometers for

meteorological applications but also for monitoring the quality of compressed air and protective gases in various factories and processes. It would be reasonable to achieve expanded uncertainty lower than 0.1 °C in the whole dew-point temperature range because the maximum permissible error of the chilled mirror hygrometer is ± 0.1 °C.

The humidity generator might work according to the two-pressure principle due to the available compressed air line in the laboratory. It will be very important to improve the temperature control of the liquid bath of the humidity generator. The temperature stability of the saturator could be improved if the saturator is immersed in a liquid bath, which temperature is directly controlled. In order to be able to calibrate relative humidity hygrometers of different sizes and configurations flexibly a temperature controlled chamber should be used.

The outcomes of the current thesis show that contamination of water in the saturator unit will not be a significant uncertainty source when constructing a humidity generator although at higher temperatures the importance of this uncertainty source may increase. Also it will probably not be necessary to put special efforts in sealing the tubing because the effect of leaks was found to be small even at frost-point temperatures of –80 °C if moderate positive gauge pressure was maintained in the tubing.

At the present moment the best measurement capability of Estonian reference standard (Figure 4) fulfils the requirements of most customers. For most of the customers it is necessary to calibrate their hygrometers at indoor conditions.

5 CONCLUSIONS

The uncertainty of relative humidity realized by the Estonian air humidity reference standard was estimated using the traditional GUM method, the MCM and the GUM method modified by the Bayesian approach. The expanded uncertainties of the methods agreed within 0.04 %rh that were about 30 to 40 times smaller than the estimated expanded uncertainties. This confirmed the reliability of uncertainty estimation. The agreement between the MCM and the Bayesian modification of the ISO GUM approach was even slightly better. For the medium relative humidity case it was necessary to use the Welch-Satterthwaite formula for calculation of the effective number of degrees of freedom in order to find the suitable Student's coefficient instead of the typical coverage factor k=2. Using the coverage factor k = 2 in such situations led to underestimation of the expanded uncertainty by up to 1.1 times.

The effect of water contamination on the dew-point temperature of air was studied in the context of humidity generators. The dew-point temperature drop due to natural contamination of water samples kept in vessels made of different materials for 2 months was found to be lower than 0.07 mK in all cases. This estimate is by more than 10 times smaller than the corresponding conservative estimates reported by several authors. This difference in the results may come from different sampling flow-rates and differences in the shape and design of saturator units and vessels used in the current study. Thus, the effect of contaminated water on the dew-point temperature drop is insignificant even nowadays while the other uncertainty components of dew-point temperature realization are decreasing. However, the purity of water in the saturator should still be addressed in uncertainty estimations and dew-point temperature realizations.

The tests with water samples intentionally contaminated with LiCl and NaCl showed good agreement between different dew-point temperature drop calculation methods and experimental dew-point temperature drop measurement results. The most frequently used calculation method based on the Raoult's law was found to be sufficiently accurate for assessing the value of dew-point temperature drop due to contamination of water in saturator units of dew-point generators.

It has been reported by several researchers that frost-point temperature uncertainty increases rapidly in the trace moisture region. It can partly be explained by water-vapour back-diffusion from ambient through leaks into the sampling line. The experiments carried out at the MIKES humidity laboratory showed that high enough leak flow-rates of dry gas (T_f = –80 °C) through circular holes in the wall of the stainless steel tubing effectively prevented water-vapour back-diffusion into the tubing. The measured critical flow-rate through circular leak holes in the wall of the tubing was found to agree well with developed simplified model for the critical flow-rate.

The measurements with loosened Swagelok and VCR connectors showed that the latter connector type was more sensitive to water-vapour back-diffusion. This can be explained by shorter effective flow-path of leaking air in the VCR connector. Leak paths of smaller cross-sectional area were found to be more potential error sources as far as water-vapour back-diffusion is concerned provided that the same positive gauge pressure is maintained in the tubing.

The results of the thesis are taken into account for developing Estonian reference standard of air humidity and the knowledge can be used for further developments.

6 SUMMARY

In 2004 the setting up of the air humidity reference standard was started by Testing Centre of University of Tartu. The acquiring of devices for setting up the secondary air humidity standard was supported by EU via Phare 2002 project "Development of Conformity Assessment Infrastructure in the Field of Metrology". The secondary standard is based on the chilled mirror dew-point hygrometer that measures the dew-point temperature or relative humidity of air that is circulating in the climatic chamber.

In 2010 the standard was named as Estonian reference standard of air humidity by a governmental decree.

This thesis is dedicated to developing Estonian reference standard of air humidity further by assessing its uncertainty components and enhancing its reliability.

Several tests have been carried out for estimating different uncertainty components of the secondary standard of air humidity. A part of these experiments have been described in the author's Master's thesis. The self-heating effect of air thermometer and the uncertainty due to radiation effects in the climatic chamber have been studied more thoroughly since these effects have not been addressed in the author's master's thesis.

Taking part in interlaboratory comparisons in the field of relative humidity and air temperature has proved that the calibration of hygrometers is reliable.

Different uncertainty estimation methods were applied to reveal potential systematic effects in the uncertainty estimation. The agreement between the traditional GUM method, the Monte Carlo Simulation method and the GUM modified by the Bayesian approach was found to be good in cases of medium and high relative humidity reference values. The corresponding expanded uncertainties agreed within 0.04 %rh. The GUM modified by Bayesian approach agreed with the MCM even better. In the case of medium relative humidity values it is necessary to use the Welch-Satterthwaite formula in order to calculate the effective number of degrees of freedom for expanded uncertainty calculation.

A simple single-pressure dew-point generator was constructed in order to monitor the stability of the reference CMH between calibrations against a primary dew-point temperature standard of a non-Estonian NMI. The dew-point generator works in a limited range of 14 °C to 19 °C. The performance tests of the dew-point generator were carried out and the expanded uncertainty of dew-point temperature generation ($k = 2$) was estimated as 0.08 °C.

The stainless steel, copper, glass and plastic (polypropylene) vessels were partly filled with ultra-high purity water in order to study the effect of natural contamination of the water samples on the corresponding dew-point temperature drops in the saturator vessels of dew-point generators. The water samples were kept in the closed vessels for 13 month and 2 month periods and in the ventilated vessels for 2 months. The largest effect in the dew-point

temperature was found in the case of ventilated copper vessel. The dew-point temperature drop was estimated as 0.07 mK when the measured contents of ions and organic compounds in this water sample as well as the corresponding expanded uncertainties were taken into account. That small effect does not significantly contribute to dew-point temperature measurement uncertainty even if the smallest expanded uncertainties of dew-point temperature generation have reduced to 20 mK.

LiCl and NaCl aqueous solutions of different concentration were used to study the methods for calculating the contamination effect on the basis of experimental data. For both types of salt solutions the dew-point temperature drops were measured with respect to high purity water. For both types of salt solutions the directly measured dew-point temperature drops were compared with the Raolt's law based calculation method and the method based on data by Fontana. For LiCl solution the dew-point temperature drops were additionally calculated using the Conde formulae. The widely used Raoult's law was found to agree well with other calculation methods as well as with direct measurement results. Therefore it is recommended to use the Raoult's law based calculation method in future due to its simplicity.

The author of the dissertation had possibility to study the effect of leaks on the frost-point temperature of very dry air in a sampling line at the MIKES humidity laboratory. It was found that maintaining positive gauge pressure in the sampling line effectively prevented water molecules from back-diffusing inside the tubing even if the frost-point temperature of air inside the tubing was as low as –80 °C.

However, leaks in slightly loosened VCR connectors were found to cause larger back-diffusion of water molecules than in Swagelok connectors due to different geometry of the connectors. It was also found that back-diffusion of water molecules into the tubing may take place more easily through leak paths of smaller cross-sectional areas.

The critical flow-rate of air that practically stops back-diffusion of water molecules through leak paths was studied experimentally and theoretically. Different diameter holes ranging from 0.05 mm to 0.5 mm were drilled in the wall of the tubing in order to model leak paths. The values of critical flow-rates of air that were calculated by diffusion and convection theories agreed well with corresponding measured values.

7 SUMMARY IN ESTONIAN

Mõõtemääramatuse allikad ja analüüsimeetodid SI õhuniiskuse ühikute realiseerimisel Eestis

Aastal 2004 alustati Tartu Ülikooli Katsekojas õhuniiskuse tugietaloni arendamist sekundaaretaloni tasemel. Selleks vajalikud seadmed soetati Euroopa Liidu toetusel Phare 2002 projekti "Development of Conformity Assessment Infrastructure in the Field of Metrology" raames. Õhuniiskuse sekundaartaseme etalon põhineb kastepunkti peegelhügromeetril, mis mõõdab kliimakambris tsirkuleeriva õhu kastepunkti temperatuuri või suhtelist niiskust.

Aastal 2010 kinnitati majandus- ja kommunikatsiooniministri määrusega TÜ Katsekojas arendatud etalon Eesti riigi õhuniiskuse tugietaloniks.

Käesolev dissertatsioon kirjeldab Eesti õhuniiskuse tugietaloni edasi arendamist, selle mõõtemääramatuse komponentide hindamist ja usaldusväärsuse tõstmist.

Kõnealuse tugietaloni mõõtemääramatuse komponentide hindamiseks on sooritatud rida eksperimente, millest osa on avaldatud autori magistritöös. Käesolevas dissertatsioonis on põhjalikumalt uuritud kliimakambris õhutermomeetri isesoojenemise mõju ja hinnatud kiirguslikest efektidest tingitud määramatust, kuna neid küsimusi ei ole varem magistritöös käsitletud.

Osalemine rahvusvahelistel võrdlusmõõtmistel õhu suhtelise niiksuse ja temperatuuri alal on objektiivselt tõendanud, et õhuniiskuse mõõturite kalibreerimine toimub usaldusväärselt.

Süstemaatiliste vigade avastamiseks on hinnatud mõõtemääramatust mitmel erineval meetodil. Suhtelise niiskuse keskmiste ja kõrgete tasemete korral on leitud referentsväärtuste hea kooskõla traditsioonilise GUM meetodi, Monte Carlo meetodi ja modifitseeritud GUM meetodi vahel. Modifitseerimiseks on kasutatud Bayesi lähenemist. Vastavad laiendmääramatused langevad kokku 0,04 %rh ulatuses. Modifitseeritud GUM meetodi ja Monte Carlo meetodi vaheline kooskõla on veelgi parem. Suhtelise niiskuse keskmistel tasemetel on vajalik kasutada Welch-Satterthwaite valemit, et arvutada efektiivne vabadusastmete arv laiendmääramatuse hindamiseks.

Lisaks peegelhügromeetri kalibreerimisele välismaistes metroloogiainstituutides, on TÜ Katsekojas peegelhügromeetri näitude kontrollimiseks konstrueeritud lihtsa ehitusega niiskusgeneraator, mis võimaldab töötamist kastepunkti temperatuuri vahemikus (14…19) °C. Seadme katsetamise ja valideerimise tulemuste alusel on hinnatud kastepunkti temperatuuri laiendmääramatuseks 0,08 °C.

Hindamaks niiskusgeneraatori küllastianuma materjali saastavat mõju vee kastepunkti temperatuurile, täideti roostevabast terasest, vasest, klaasist ja plastikust anumad poolenisti veega, mille puhtusaste oli väga kõrge. Ühes eksperimendis hoiti veeproove suletud anumates 13 kuu vältel ja korduskatses veel 2 kuu vältel. Teises eksperimendis hoiti kahe kuu vältel samasuguse

puhtusastmega vett ventileeritavates anumates. Suurim kastepunkti temperatuuri langus leidis aset ventileeritavas vaskanumas. Selle kastepunkti temperatuuri languse väärtuseks saadi halvima juhu meetodil 0,07 mK, juhul kui võeti arvesse ioonide ja orgaaniliste ühendite tegelikult mõõdetud sisaldust ja lisati mõõtemääramatus. Nii väike saastumise efekt ei anna olulist panust kastepunkti temperatuuri mõõtemääramatusele isegi juhul, kui kastepunkti temperatuuri realiseerimise laiendmääramatus on tänapäevasel tipptasemel 20 mK.

Valmistati ka erineva kontsentratsiooniga LiCl ja NaCl lahuseid, et uurida vee saastumisest tingitud kastepunkti temperatuuri languse arvutamise meetodeid. Mõlema soolalahuse korral mõõdeti kastepunkti temperatuuri languseid puhta deioniseeritud vee suhtes. Eksperimentaalseid tulemusi võrreldi Raoulti seadusel põhineva arvutusmeetodi ja nõndanimetatud Fontana meetodi kaudu arvutatud vastavate väärtustega. Lisaks sellele arvutati LiCl lahuse korral kastepunkti temperatuuri langus, kasutades Conde valemeid. Tavapäraselt kasutatav Raoulti meetod andis tulemusi, mis langesid hästi kokku teiste arvutusmeetoditega ja ka otseselt mõõdetud tulemustega. Eksperimendi tulemusena võib soovitada Raoulti seadusel põhinevat arvutusmeetodit kasutada ka tulevikus tänu selle lihtsusele.

MIKES-i õhuniiskuse laboris oli autoril võimalus uurida väga kuiva õhu puhul torulekete mõju torus voolava õhu härmapunkti temperatuurile. Uurimise käigus leiti, et kui voolava õhu rõhk ületab toru ümbritsevat atmosfäärirõhku, siis õhus leiduvate veemolekulide tagasidifusioon (väljastpoolt toru sisse) on takistatud isegi siis, kui torus voolab väga kuiv õhk (eksperimendis oli õhu härmapunkti temperatuur –80 °C).

Vee molekulide tagasidifusioon läbi kergelt vabastatud VCR toruliitmike leiti olevat märgatavam tagasidifusioonist läbi Swageloki liitmike, kuna nende liitmike kuju ja mõõtmed on üksteisest erinevad. Uurimise käigus leiti samuti, et veemolekulide tagasidifusioon toru sisemusse võib toimuda väiksema ristlõike pindalaga lekkekohtade kaudu hõlpsamini.

Nõndanimetatud kriitilist õhuvoogu, mis praktiliselt peatab veemolekulide tagasidifusiooni läbi lekkekohtade, uuriti eksperimentaalselt ja teooria alusel. Lekkekohtade modelleerimiseks puuriti toru seina erineva läbimõõduga avad vahemikus (0,05...0,5) mm. Difusiooni- ja konvektsiooniteooriate alusel arvutatud kriitilised õhuvoo väärtused ja eksperimentaalsed väärtused langesid hästi kokku.

8 APPENDIX I

Table A1 Uncertainty budget for the medium relative humidity case using equations 2.4 and 3.1 to 3.3

Quantity	Value	Probability density function	Standard uncer-tainty, u_i	Sensitivity coefficient c_i	(c_i*u_i)/ %rh	Contribu-tion
K [a]	1	Rectang.	0.0004	54 %rh	0.0216	0.1%
$T_d(average)$	288 K	Student's	0.2 K	3.5 %rh K^{-1}	0.7	80.3%
$\Delta T_{d,corr}$	0.05 K	Normal	0.04 K	3.5 %rh K^{-1}	0.14	3.2%
$\Delta T_{d,p}$	0.03 K	Rectang.	0.0058 K	3.5 %rh K^{-1}	0.0203	0.1%
$\delta T_{d,approx}$	0 K	Normal	0.02 K	3.5 %rh K^{-1}	0.07	0.8%
$\delta T_{d,drift}$	0 K	Rectang.	0.0115 K	3.5 %rh K^{-1}	0.04025	0.3%
$\delta T_{d,hom}$	0 K	Rectang.	0.058 K	3.5 %rh K^{-1}	0.203	6.7%
$\delta T_{d,res}$	0 K	Rectang.	0.0029 K	3.5 %rh K^{-1}	0.01015	0.0%
$T(average)$	297.98 K	Student's	0.02 K	–3.2 %rh K^{-1}	–0.064	0.7%
ΔT_{corr}	–0.02 K	Normal	0.02 K	–3.2 %rh K^{-1}	–0.064	0.7%
ΔT_{selfh}	–0.05 K	Rectang.	0.0173 K	–3.2 %rh K^{-1}	–0.05536	0.5%
δT_{approx}	0 K	Normal	0.02 K	–3.2 %rh K^{-1}	–0.064	0.7%
δT_{drift}	0 K	Rectang.	0.0115 K	–3.2 %rh K^{-1}	–0.0368	0.2%
δT_{hom}	0 K	Rectang.	0.058 K	–3.2 %rh K^{-1}	–0.1856	5.6%
δT_{res}	0 K	Rectang.	0.0029 K	–3.2 %rh K^{-1}	–0.00928	0.0%
δT_{rad}	0 K	Rectang.	0.0115 K	–3.2 %rh K^{-1}	–0.0368	0.2%
$\delta E_w(T_d)$	1	Normal	0.00005	150 %rh	0.0075	0.0%
$\delta E_w(T)$	1	Normal	0.00005	–190 %rh	–0.0095	0.0%
h_{ref}	**54.34 %rh**				0.781	
$U(h_{ref})$					**1.72**	
v_{eff}	14					
t	2.20					

[a] K takes into account omitted enhancement factors in equation 2.4.

Table A2 Uncertainty budget for the high relative humidity case using equations 2.4 and 3.1 to 3.3

Quantity	Value	Probability density function	Standard uncer-tainty, u_i	Sensitivity coefficient c_i	(c_i*u_i)/ %rh	Contri-bution
K [a]	1	Rectang.	0.0004	90 %rh	0.036	0.3%
$T_d(average)$	296 K	Student's	0.05 K	5.4 %rh K^{-1}	0.27	19.0%
$\Delta T_{d,corr}$	0.05 K	Normal	0.04 K	5.4 %rh K^{-1}	0.216	12.1%
$\Delta T_{d,p}$	0.03 K	Rectang.	0.0058 K	5.4 %rh K^{-1}	0.03132	0.3%
$\delta T_{d,approx}$	0 K	Normal	0.02 K	5.4 %rh K^{-1}	0.108	3.0%
$\delta T_{d,drift}$	0 K	Rectang.	0.0115 K	5.4 %rh K^{-1}	0.0621	1.0%
$\delta T_{d,hom}$	0 K	Rectang.	0.058 K	5.4 %rh K^{-1}	0.3132	25.5%
$\delta T_{d,res}$	0 K	Rectang.	0.0029 K	5.4 %rh K^{-1}	0.01566	0.1%
$T(average)$	297.98 K	Student's	0.02 K	–5.4 %rh K^{-1}	–0.108	3.0%
ΔT_{corr}	–0.02 K	Normal	0.02 K	–5.4 %rh K^{-1}	–0.108	3.0%
ΔT_{selfh}	–0.05 K	Rectang.	0.0173 K	–5.4 %rh K^{-1}	–0.09342	2.3%
δT_{approx}	0 K	Normal	0.02 K	–5.4 %rh K^{-1}	–0.108	3.0%
δT_{drift}	0 K	Rectang.	0.0115 K	–5.4 %rh K^{-1}	–0.0621	1.0%
δT_{hom}	0 K	Rectang.	0.058 K	–5.4 %rh K^{-1}	–0.3132	25.5%
δT_{res}	0 K	Rectang.	0.0029 K	–5.4 %rh K^{-1}	–0.01566	0.1%
δT_{rad}	0 K	Rectang.	0.0115 K	–5.4 %rh K^{-1}	–0.0621	1.0%
$\delta E_w(T_d)$	1	Normal	0.00005	300 %rh	0.015	0.1%
$\delta E_w(T)$	1	Normal	0.00005	–310 %rh	–0.0155	0.1%
h_{ref}	**89.58**				0.620	
$U(h_{ref})$					**1.24**	
v_{eff}	240					
t	2.00					

[a] K takes into account omitted enhancement factors in equation 2.4.

9 REFERENCES

1. T. Quinn, J. Kovalevsky. The Development of Modern Metrology and Its Role Today. *Phil. Trans. R. Soc. A.*, **2005**, 363, 2307–2327.
2. Development of Conformity Assessment Infrastructure in the Field of Metrology; Donor: PHARE, Reference: EuropeAid/113156/D/SV/EE, 2002–2004, Budget EUR: 3 343 300, Project Coordination: Ministry of Economic Affairs.
3. S. Bell, The expanding horizons of humidity measurement. *TEMPMEKO 1999: 7th International Symposium on Temperature and Thermal Measurement in Industry and Science, Proceedings* **1999**, Vol. 1, 11–18.
4. M. Stevens, R. Benyon. Conceptual design of a low-range humidity standard generator. *ISHM, 1998: 3rd International Symposium on Humidity & Moisture, Proceedings*, **1998** 103–110.
5. A. Wexler. Humidity and Moisture. Measurement Control in Science and Industry. New York, Reinhold Publishing Corp., **1965**, Vol. III.
6. L. Greenspan. Functional equations for the enhancement factors for CO_2 – free moist air. *J. Res. NBS*, **1975**, 80A, 41–44.
7. D. Sonntag. Important new values of the physical constants of 1986, vapour pressure formulations based on the ITS-90 and psychrometer formulae. *Meteorol. Zeitschrift*, **1990**, 70, 340–344.
8. A Guide to the Measurement of Humidity, NPL, London, **1996.**
9. P. R. Wiederhold. Water Vapor Measurement, New York, Marcel Dekker Inc., **1997**.
10. M. Heinonen, Uncertainty in humidity measurements. *Publication of the EUROMET Workshop P758*, Mittatekniikan Keskus, **2006**.
11. M. Stevens, S. Bell. The Humidity Facility at the UK National Physical Laboratory. *ISHM 2002: 4th International Symposium on Humidity & Moisture, Proceedings*, **2002**, 2–9.
12. A. Actis, S. Bell, R. Benyon, B. Cretinon, M. de Groot, M. Heinonen, G. Scholz, A. Steiner. The use of a humid air generator as a reference method for measuring humidity. *ISHM* 1998: *3rd International Symposium on Humidity & Moisture, Proceedings*, **1998**, 10–19.
13. C. W. Meyer, J. T. Hodges, R. W. Hyland, G. E. Scace, J. Valencia-Rodriguez, J. R. Whetstone. The second-generation NIST standard hygrometer. *Metrologia*, **2010**, 47, 192–207.
14. D. Hudoklin, J. Drnovšek. The New LMK Primary Standard for Dew-point Sensor Calibration: Evaluation of the High-Range Saturator Efficiency. *Int J Thermophys*, **2008**, 29, 1652–1659.
15. M. Heinonen. Report to the CCT on Key Comparison on EUROMET.T-K6 (EUROMET Project no. 621) Comparison of the realisations of local dew/frost-point temperature scales in the range –50 °C to +20 °C. *Metrologia*, **2010**, 47.
16. H. Abe, H. Kitano. Development of humidity standard in trace moisture region: characteristics of humidity generation of diffusion tube humidity generator. *Sensors and Actuators A*, **2006**, 128, 202–208.
17. The scale of relative humidity of air certified against saturated salt solutions, OIML R 121, **1996**.
18. JCGM 200:2008. International vocabulary of metrology – Basic and general concepts and associated terms (VIM), **2008**.

19. JCGM 100:2008. Evaluation of measurement data – Guide to the expression of uncertainty in measurement, **2008**.
20. P. Huang. Determining uncertainties in standard dew/frost-point generators for humidity measurements. *TEMPMEKO 1996: 6th International Symposium on Temperature and Thermal Measurement in Industry and Science, Proceedings*, **1996**, 577–582.
21. P. Huang. Determining the uncertainties of relative humidity, dew/frost-point temperature and mixing ratio in a humidity standard generator. *ISHM 1998*: 3rd *International Symposium on Humidity & Moisture, Proceedings*, **1998**, 149–158.
22. J. Lovell-Smith. The propagation of uncertainty for humidity calculations. *Metrologia*, **2009**, 46, 607–615.
23. G. Wübbeler, M. Krystek, C. Elster. Evaluation of measurement uncertainty and its numerical calculation by a Monte Carlo method. *Meas. Sci. Technol*, **2008**, 19.
24. JCGM 101:2008, Evaluation of measurement data – Supplement 1 to the "Guide to the expression of uncertainty in measurement" – Propagation of distributions using a Monte Carlo method, **2008**.
25. M. A. Herrador, A. G. Asuero, A. G. Gonzalez. Estimation of the uncertainty of indirect measurements from the propagation of distributions by using the Monte-Carlo method: An overview. *Chemometrics and Intelligent Laboratory Systems*, **2005**, 79, 115–122.
26. M. A. Herrador, A. G. Gonzalez. Evaluation of measurement uncertainty in analytical assays by means of Monte Carlo simulation. *Talanta*, **2004**, 64, 415–422.
27. A. G. Gonzalez, M. A. Herrador, A. G. Asuero. Uncertainty evaluation from Monte-Carlo simulations by using Crystal-Ball software. *Accred Qual Assur*, **2005**, 10, 149–154.
28. M. Cox, P. Harris, B. R.-L. Siebert. Evaluation of measurement uncertainty based on the propagation of distributions using Monte Carlo simulation. *Measurement Techniques*, **2003**, 46, 824–833.
29. M. G. Cox, B. R.-L. Siebert. The use of a Monte Carlo method for evaluating uncertainty and expanded uncertainty. *Metrologia*, **2006**, 43, S178–S188.
30. V. Carpentier, M. Megharfi, J. Quint, M. Priel, M. Desenfant, R. Morice. Estimation of hygrometry uncertainties by propagation of distributions. *Metrologia*, **2004**, 41, 432–438.
31. R. N. Kacker. Bayesian alternative to the ISO-GUM's use of the Welch-Satterthwaite formula. *Metrologia*, **2006**, 43, 1–11.
32. R. N. Kacker, A. T. Jones. On use of Bayesian statistics to make the Guide to the Expression of Uncertainty in Measurement consistent. *Metrologia*, **2003**, 40, 235–248.
33. R. N. Kacker, B. Toman, D. Huang. Comparison of ISO-GUM, draft GUM Supplement 1 and Bayesian statistics using simple linear calibration. *Metrologia*, **2006**, 43, S167–S177.
34. M. Stevens, S. A. Bell. The NPL standard humidity generator: an analysis of uncertainty by validation of individual component performance. *Meas. Sci. Technol.*, **1992**, 3, 943–952.
35. M. Heinonen. Validation of the MIKES primary dew-point generator. Julkaisu J1. **1997**, Centre for Metrology and Accreditation.
36. J. Nielsen, M. J. de Groot. Revision and uncertainty evaluation of a primary dewpoint generator. *Metrologia*, **2004**, 41, 167–172.

37. H. Kitano, T. Niwa, N. Ochi, C. Takahashi. Saturator efficiency and uncertainty of NMIJ two-pressure two-temperature humidity generator, *Int J Thermophys,* **2008**, 29, 1615–1622.
38. C. W. Meyer, W. W. Miller, D. C. Ripple, G. E. Scace. Performance and validation tests on the NIST hybrid humidity generator. *Int J Thermophys*, **2008**, 29, 1606–1614.
39. H. G. Liedberg, M. R. Mnguni, D. Jonker. A simple humidity generator for relative humidity calibrations. *Int J Thermophys*, **2008**, 29, 1660–1667.
40. R. Bosma, D. Mutter, A. Peruzzi. Validation of a dew-point generator for pressures up to 6 MPa using nitrogen and air. *Metrologia*, **2012**, 49, 597–606.
41. C. W. Meyer, W. W. Miller, D. C. Ripple, G. E. Scace. Uncertainty budget for the NIST hybrid humidity generator. *Int J Thermophys*, **2012**, 33, 1488–1499.
42. D. Zvizdic, M. Heinonen, D. Sestan. New primary dew-point generators at HMI/FSB-LPM in the range from –70 °C to +60 °C. *Int J Thermophys*, **2012**, 33, 1536–1549.
43. B. I. Choi, J. C. Kim, S. B. Woo. Uncertainty of the Kriss low frost-point humidity generator. *Int J Thermophys*, **2012**, 33, 1559–1567.
44. R. Benyon, T. Vicente. Consistency of the national realization of dew-point temperature using standard humidity generators. *Int J Thermophys*, **2012**, 33, 1550–1558.
45. D. Hudoklin, J. Bojkovski, J. Nielsen, J. Drnovšek. Design and validation of a new primary standard for calibration of the top-end humidity sensors. *Measurement*, **2008**, 41, 950–959.
46. M. Heinonen. National basis for traceability in humidity measurements. *Thesis for the degree of Doctor of Technology*, Helsinki University of Technology, **1999**.
47. A. Actis, M. Banfo, V.C. Fernicola, R. Galleano, S. Merlo. Metrological performances of the IMGC two-temperature primary humidity generator for the temperature range –15 °C to 90 °C. *ISHM 1998*: 3rd *International Symposium on Humidity & Moisture, Proceedings*, **1998**, 2–9.
48. B. Cretinon. The CETIAT standard humidity generator operating from –60 °C to +70 °C in dew point temperature. *ISHM 1998*: 3rd *International Symposium on Humidity & Moisture, Proceedings*, **1998**, 45–51.
49. B. Blanquart, B. Cretinon, Y. Hermier. Improvement of CETIAT Humidity Generator for Dew/Frost-Point in a Range from –80 °C up to +15 °C. *ISHM 2002*: 4th *International Symposium on Humidity & Moisture, Proceedings*, **2002** 26–32.
50. C. Takahashi, H. Kitano, N. Ochi. Uncertainty and performance of the NRLM two-pressure and two-temperature humidity generator. *TEMPMEKO 1999*: 7th *International Symposium on Temperature and Thermal Measurement in Industry and Science, Proceedings*, **1999**, Vol. 1, 197–202.
51. D. Zvizdic, V. Kolobaric, I. Galaso, D. Serfezi. A new two temperature humidity generator as a primary standard for measuring humidity in Croatia. *TEMPMEKO 1999*: 7th *International Symposium on Temperature and Thermal Measurement in Industry and Science, Proceedings*, **1999**, Vol. 1, 203–208.
52. K. Flakiewicz. Implementation of the dew-point temperature generator as the primary standard in GUM. *ISHM 1998: 3rd International Symposium on Humidity & Moisture, Proceedings*, **1998**, 62–67.
53. K. Flakiewicz. Improvement of the primary humidity standard in GUM. *TEMPMEKO 2001*: 8th *International Symposium on Temperature and Thermal Measurement in Industry and Science, Proceedings*, **2002,** Vol. 1, 579–582.

54. V. C. Fernicola, M. Banfo. The humidity facility for hygrometer calibration at the IMGC-CNR. *TEMPMEKO 2001*: 8th *International Symposium on Temperature and Thermal Measurement in Industry and Science, Proceedings*, **2002**, Vol. 2, 751–756.
55. R. Benyon, R. F. Pragnell. Development of the Spanish national humidity standard facility. *ISHM 1998*: 3rd *International Symposium on Humidity & Moisture, Proceedings*, **1998**, 37–44.
56. P. Reinshaus, B. Werner. Using a two-temperature – two-pressure humidity generator for the in-situ calibration of chilled mirror hygrometers for a wide temperature range. *TEMPMEKO 2001: 8th International Symposium on Temperature and Thermal Measurement in Industry and Science, Proceedings*, **2002**, Vol. 1, 351–356.
57. H. Mitter. The BEV/E+E Elektronik standard humidity generator. *ISHM 2006: 5th International Symposium on Humidity & Moisture*, Proceedings, **2006**.
58. P Mackrodth, R. Benyon, G. Scholz. State-of-the-art calibration of high-range chilled-mirror hygrometers and their use in the intercomparison of humidity standard generators, *ISHM 1998: 3rd International Symposium on Humidity & Moisture*, Proceedings, **1998**, 159–166.
59. B. Hardy. Trust but verify – practical approaches to humidity generation and measurement. *TEMPMEKO 2004*: 9th *International Symposium on Temperature and Thermal Measurement in Industry and Science, Proceedings*, **2004**, Vol. 1, 23–32.
60. J. Nielsen, M. J. de Groot. A new set-up for the generation of humidity in the ppb range. *TEMPMEKO 2001*: 8th *International Symposium on Temperature and Thermal Measurement in Industry and Science, Proceedings*, **2002**, Vol. 1, 345–350.
61. M. Heinonen, et al. Investigation of the equivalence of national dew-point temperature realizations in the range –50 °C to +20 °C. *Int J Thermophys*, 2010, 10.1007/s10765-011-0950-x.
62. N. K. Verma, A. M. Haider, F. Shadman. Contamination of ultrapure systems by back-diffusion of gaseous impurities. *J. Electrochem. Soc.*, **1993**, 140, 1459–1463.
63. T-S. Yang, C-H. Wu, C-F. Yeh. Analysis of moisture purge in high purity gas distribution systems. *International Journal of Heat and Mass Transfer*, **2006**, 49, 1753–1759.
64. M. Stevens, F. Hussain, S. A. Bell, H. Othman, Md. Nor Md. Chik, R. Gee. An investigation of the drying response time of sample lines made from different materials. ISHM 2006: *5th International Symposium on Humidity & Moisture, Proceedings*, **2006**.
65. F. Hussain, S Khairuddin, H. Othman, Md. Nor, Md.Chik. Facilities for humidity calibration at National Metrology Laboratory (NML), Malaysia. *ISHM 2006: 5th International Symposium on Humidity and Moisture*, *Proceedings*, **2006**.
66. GUIDELINE DKD-R 5–7, Calibration of Climatic Chambers, **2009**.
67. C. Rauta, F. Helgesen, T. Magnussen. Investigation of the measurement uncertainty in a climatic chamber used for calibration of the RH sensors. *TEMPMEKO 2001: 8th International Symposium on Temperature and Thermal Measurement in Industry and Science, Proceedings,* **2002**, Vol. 2, 917–922.
68. L.A. Lima, A.F. Orlando. Contributions to the uncertainty of humidity measurement of the temperature uniformity in a climatic test chamber. *ISHM 2006:5th International Symposium on Humidity & Moisture, Proceedings,* **2006**.

69. J. Bojkovski, D. Hudoklin, I. Pušnik. Custom-made automated system for evaluation of climatic chambers. *ISHM 2006:5th International Symposium on Humidity & Moisture, Proceedings,* **2006**.
70. S. Friederici, E. Tegeler. Radiation effects and its consequences on measurements in climatic chambers. *TEMPMEKO 2004: 9th International symposium on temperature and thermal measurement in industry and science, Proceedings*, **2004**, Vol. 2, 795–800.
71. V. Žužek, V. Batagelj, J. Bojkovski. Determination of PRT Hysteresis in the Temperature Range from –50 °C to 300 °C. *Int J Thermophys*, **2010**, 31, 1771–1778.
72. D. R. White, C. L. Jongelenen, P. Saunders. The Hysteresis Characteristics of Some Industrial PRTs. *Int J Thermophys*, **2010**, 31, 1676–1684.
73. R. Benyon, J. Lovell-Smith, R. Mason, T. Vicente. State-of-the-art calibration of relative humidity sensors. *TEMPMEKO 2001: 8th International symposium on temperature and thermal measurement in industry and science, Proceedings*, **2002**, Vol.2, 1003–1008.
74. M. Vilbaste. Master's thesis, **2005**, University of Tartu (in Estonian).
75. D. Sonntag. Advancements in the field of hygrometry. *Meteorol. Zeitschrift*, **1994**, 3, 51–66.
76. M. Heinonen. Simplified methods to calculate the dew-point temperature change due to a pressure drop, *Tempmeko 2001: 8th International symposium on temperature and thermal measurement in industry and science, Proceedings*, **2002**, Vol. 2, 609–614.
77. Conde-Petit M R, Aqueous solutions of lithium and calcium chlorides: Property formulations for use in air conditioning equipment design, **2009**, M. Conde Engineering.
78. Barbosa-Canovas G V, Fontana A J Jr., Schmidt S J and Labuza T P, **2007**, *Water Activity in Foods: Fundamentals and Applications*, John Wiley & Sons.
79. F. P. Incropera, et al. Fundamentals of Heat and Mass Transfer, Wiley, **2007**, 6th edition.
80. M. Heinonen, et al. EURAMET P1061 – Comparison of air temperature calibrations, Final report, **2013**, MIKES.

ACKNOWLEDGEMENT

At first I would like to thank my three supervisors. I am very grateful to Dr. Olev Saks who has taught me the basics about metrology and continually helps me in everyday work for developing the Estonian air humidity and air velocity standards. I admire his enthusiasm at his high age. I thank Dr. Martti Heinonen and professor Ivo Leito for agreeing to be my supervisors while being very busy researchers. Dr. Martti Heinonen has trained me for setting up the air humidity standard and we have cooperated in research. I thank him for this and for his hospitality during my stay at MIKES. I am very grateful to professor Ivo Leito for encouraging me to complete my studies as well as for supporting me in research and everyday work.

I thank Vladimir Šor, Leo Visberg and Viljar Pihl for their help in constructing experimental set-up, Hannu Räsänen and Sampoo Sillanpää for helping me in practical matters at MIKES, Urmas Muinasmaa for ICP-MS analysis and Georgi Slavin for developing the Monte Carlo simulation software.

I am grateful to my colleagues at the analytical chemistry department for creating a good working atmosphere. I would especially like to thank associate professor Koit Herodes and Karin Kipper for being very helpful persons.

I would like to thank Riho Vendt, Viktor Vabson and Toomas Kübarsepp for extending my general knowledge about metrology and for their will to help me.

I am greatly indebted to lecturers at the Institute of Physics for teaching me this difficult subject.

Finally I would like to thank my parents, relatives and friends for supporting me.

PUBLICATIONS

CURRICULUM VITAE

Name:	Martin Vilbaste
Born:	05.01.1979, Tallinn, Estonia
Citizenship:	Estonian
Address:	University of Tartu, Institute of Chemistry, Ravila 14a, 50411 Tartu, Estonia
E-mail:	martin.vilbaste@ut.ee

Education

2005–…	University of Tartu, PhD student
2002–2005	University of Tartu, MSc(applied physics)
1997–2002	University of Tartu, BSc(physics)

Professional emlpoyment

2010–…	University of Tartu, Institute of Chemistry, research fellow
2008–2010	University of Tartu, Institute of Chemistry, engineer
2002–2008	University of Tartu, Faculty of Physics and Chemistry, engineer

Supervised dissertations

2011	Cagatay Ipbüker, MSc, (sup) Tõnu Mauring, (sup) Martin Vilbaste, "Air Change Rate of Buildings. A Case Study", University of Tartu

Other activities

EURAMET TC-Therm (European Association of National Metrology Institutes, Technical Committee for Thermometry), Humidity sub-committee, contact person of Estonia

Publications

1. C. Ipbüker, M. Valge, M. Vilbaste, T. Mauring, A-H. Tkaczyk, Uncertainty evaluation of single-point fan pressurization measurements for calm and assumed windy conditions, Fresenius Environmental Bulletin, 23(6), (2014), 1529–1538.
2. M. Vilbaste, M. Heinonen, O. Saks, I. Leito, The effect of water contamination on the dew-point temperature scale realization with humidity generators, Metrologia, 50, (2013), 329–336.
3. M. Vilbaste, G. Slavin, O. Saks, V. Pihl, I. Leito, Can coverage factor 2 be interpreted as an equivalent to 95% coverage level in uncertainty estimation? Two case studies, Measurement, 43(3), (2010), 392–399.
4. M. Heinonen, M. Vilbaste, Frost-Point Measurement Error Due to a Leak in a Sampling Line, International Journal of Thermophysics, 29(5), (2008), 1589–1597.

5. A. Rodima, M. Vilbaste, O. Saks, E. Jakobson, E. Koort, V. Pihl, L. Sooväli, L. Jalukse, J. Traks, K. Virro, H. Annuk, K. Aruoja, A. Floren, E. Indermitte, M. Jurgenson, P. Kaleva, K. Kepler, I. Leito, (2005). ISO 17025 quality system in a university environment, Accreditation and Quality Assurance, 10(7), (2005), 369–372.

ELULOOKIRJELDUS

Nimi:	Martin Vilbaste
Sünniaeg :	05.01.1979, Tallinn, Eesti
Kodakondsus:	Eesti
Aadress:	Tartu Ülikool, Keemia Instituut, Ravila 14a, 50411 Tartu, Eesti
E-post:	martin.vilbaste@ut.ee

Haridustee

2005–…	Tartu Ülikool, doktorant
2002–2005	Tartu Ülikool, MSc(rakendusfüüsika)
1997–2002	Tartu Ülikool, BSc(füüsika)

Teenistuskäik

2010–…	Tartu Ülikool, Keemia Instituut, erakorraline teadur
2008–2010	Tartu Ülikool, Keemia Instituut, insener
2002–2008	Tartu Ülikool, Füüsika-keemiateaduskond, insener

Juhendatud dissertatsioonid

2011	Cagatay Ipbüker, MSc, juhendajad Tõnu Mauring ja Martin Vilbaste, “Air Change Rate of Buildings. A Case Study”, Tartu Ülikool

Muu tegevus Eesti kontaktisik EURAMETi Temperatuuri tehnilise komitee niiskuse alakomitees

Publikatsioonid

1. C. Ipbüker, M. Valge, M. Vilbaste, T. Mauring, A-H. Tkaczyk, Uncertainty evaluation of single-point fan pressurization measurements for calm and assumed windy conditions, Fresenius Environmental Bulletin, 23(6), (2014), 1529–1538.
2. M. Vilbaste, M. Heinonen, O. Saks, I. Leito, The effect of water contamination on the dew-point temperature scale realization with humidity generators, Metrologia, 50, (2013), 329–336.
3. M. Vilbaste, G. Slavin, O. Saks, V. Pihl, I. Leito, Can coverage factor 2 be interpreted as an equivalent to 95% coverage level in uncertainty estimation? Two case studies, Measurement, 43(3), (2010), 392–399.
4. M. Heinonen, M. Vilbaste, Frost-Point Measurement Error Due to a Leak in a Sampling Line, International Journal of Thermophysics, 29(5), (2008), 1589–1597.
5. A. Rodima, M. Vilbaste, O. Saks, E. Jakobson, E. Koort, V. Pihl, L. Sooväli, L. Jalukse, J. Traks, K. Virro, H. Annuk, K. Aruoja, A. Floren, E. Indermitte, M. Jurgenson, P. Kaleva, K. Kepler, I. Leito, (2005). ISO 17025 quality system in a university environment, Accreditation and Quality Assurance, 10(7), (2005), 369–372.

DISSERTATIONES PHYSICAE UNIVERSITATIS TARTUENSIS

1. **Andrus Ausmees.** XUV-induced electron emission and electron-phonon interaction in alkali halides. Tartu, 1991.
2. **Heiki Sõnajalg.** Shaping and recalling of light pulses by optical elements based on spectral hole burning. Tartu, 1991.
3. **Sergei Savihhin.** Ultrafast dynamics of F-centers and bound excitons from picosecond spectroscopy data. Tartu, 1991.
4. **Ergo Nõmmiste.** Leelishalogeniidide röntgenelektronemissioon kiiritamisel footonitega energiaga 70–140 eV. Tartu, 1991.
5. **Margus Rätsep.** Spectral gratings and their relaxation in some low-temperature impurity-doped glasses and crystals. Tartu, 1991.
6. **Tõnu Pullerits.** Primary energy transfer in photosynthesis. Model calculations. Tartu, 1991.
7. **Olev Saks.** Attoampri diapasoonis voolude mõõtmise füüsikalised alused. Tartu, 1991.
8. **Andres Virro.** AlGaAsSb/GaSb heterostructure injection lasers. Tartu, 1991.
9. **Hans Korge.** Investigation of negative point discharge in pure nitrogen at atmospheric pressure. Tartu, 1992.
10. **Jüri Maksimov.** Nonlinear generation of laser VUV radiation for high-resolution spectroscopy. Tartu, 1992.
11. **Mark Aizengendler.** Photostimulated transformation of aggregate defects and spectral hole burning in a neutron-irradiated sapphire. Tartu, 1992.
12. **Hele Siimon.** Atomic layer molecular beam epitaxy of A^2B^6 compounds described on the basis of kinetic equations model. Tartu, 1992.
13. **Tõnu Reinot.** The kinetics of polariton luminescence, energy transfer and relaxation in anthracene. Tartu, 1992.
14. **Toomas Rõõm.** Paramagnetic H^{2-} and F^+ centers in CaO crystals: spectra, relaxation and recombination luminescence. Tallinn, 1993.
15. **Erko Jalviste.** Laser spectroscopy of some jet-cooled organic molecules. Tartu, 1993.
16. **Alvo Aabloo.** Studies of crystalline celluloses using potential energy calculations. Tartu, 1994.
17. **Peeter Paris.** Initiation of corona pulses. Tartu, 1994.
18. **Павел Рубин.** Локальные дефектные состояния в CuO_2 плоскостях высокотемпературных сверхпроводников. Тарту, 1994.
19. **Olavi Ollikainen.** Applications of persistent spectral hole burning in ultrafast optical neural networks, time-resolved spectroscopy and holographic interferometry. Tartu, 1996.
20. **Ülo Mets.** Methodological aspects of fluorescence correlation spectroscopy. Tartu, 1996.
21. **Mikhail Danilkin.** Interaction of intrinsic and impurity defects in CaS:Eu luminophors. Tartu, 1997.

22. **Ирина Кудрявцева.** Создание и стабилизация дефектов в кристаллах KBr, KCl, RbCl при облучении ВУФ-радиацией. Тарту, 1997.
23. **Andres Osvet.** Photochromic properties of radiation-induced defects in diamond. Tartu, 1998.
24. **Jüri Örd.** Classical and quantum aspects of geodesic multiplication. Tartu, 1998.
25. **Priit Sarv.** High resolution solid-state NMR studies of zeolites. Tartu, 1998.
26. **Сергей Долгов.** Электронные возбуждения и дефектообразование в некоторых оксидах металлов. Тарту, 1998.
27. **Kaupo Kukli.** Atomic layer deposition of artificially structured dielectric materials. Tartu, 1999.
28. **Ivo Heinmaa.** Nuclear resonance studies of local structure in $RBa_2Cu_3O_{6+x}$ compounds. Tartu, 1999.
29. **Aleksander Shelkan.** Hole states in CuO_2 planes of high temperature superconducting materials. Tartu, 1999.
30. **Dmitri Nevedrov.** Nonlinear effects in quantum lattices. Tartu, 1999.
31. **Rein Ruus.** Collapse of 3d (4f) orbitals in 2p (3d) excited configurations and its effect on the x-ray and electron spectra. Tartu, 1999.
32. **Valter Zazubovich.** Local relaxation in incommensurate and glassy solids studied by Spectral Hole Burning. Tartu, 1999.
33. **Indrek Reimand.** Picosecond dynamics of optical excitations in GaAs and other excitonic systems. Tartu, 2000.
34. **Vladimir Babin.** Spectroscopy of exciton states in some halide macro- and nanocrystals. Tartu, 2001.
35. **Toomas Plank.** Positive corona at combined DC and AC voltage. Tartu, 2001.
36. **Kristjan Leiger.** Pressure-induced effects in inhomogeneous spectra of doped solids. Tartu, 2002.
37. **Helle Kaasik.** Nonperturbative theory of multiphonon vibrational relaxation and nonradiative transitions. Tartu, 2002.
38. **Tõnu Laas.** Propagation of waves in curved spacetimes. Tartu, 2002.
39. **Rünno Lõhmus.** Application of novel hybrid methods in SPM studies of nanostructural materials. Tartu, 2002.
40. **Kaido Reivelt.** Optical implementation of propagation-invariant pulsed free-space wave fields. Tartu, 2003.
41. **Heiki Kasemägi.** The effect of nanoparticle additives on lithium-ion mobility in a polymer electrolyte. Tartu, 2003.
42. **Villu Repän.** Low current mode of negative corona. Tartu, 2004.
43. **Алексей Котлов.** Оксианионные диэлектрические кристаллы: зонная структура и электронные возбуждения. Tartu, 2004.
44. **Jaak Talts.** Continuous non-invasive blood pressure measurement: comparative and methodological studies of the differential servo-oscillometric method. Tartu, 2004.
45. **Margus Saal.** Studies of pre-big bang and braneworld cosmology. Tartu, 2004.

46. **Eduard Gerškevitš.** Dose to bone marrow and leukaemia risk in external beam radiotherapy of prostate cancer. Tartu, 2005.
47. **Sergey Shchemelyov.** Sum-frequency generation and multiphoton ionization in xenon under excitation by conical laser beams. Tartu, 2006.
48. **Valter Kiisk.** Optical investigation of metal-oxide thin films. Tartu, 2006.
49. **Jaan Aarik.** Atomic layer deposition of titanium, zirconium and hafnium dioxides: growth mechanisms and properties of thin films. Tartu, 2007.
50. **Astrid Rekker.** Colored-noise-controlled anomalous transport and phase transitions in complex systems. Tartu, 2007.
51. **Andres Punning.** Electromechanical characterization of ionic polymer-metal composite sensing actuators. Tartu, 2007.
52. **Indrek Jõgi.** Conduction mechanisms in thin atomic layer deposited films containing TiO_2. Tartu, 2007.
53. **Aleksei Krasnikov.** Luminescence and defects creation processes in lead tungstate crystals. Tartu, 2007.
54. **Küllike Rägo.** Superconducting properties of MgB_2 in a scenario with intra- and interband pairing channels. Tartu, 2008.
55. **Els Heinsalu.** Normal and anomalously slow diffusion under external fields. Tartu, 2008.
56. **Kuno Kooser.** Soft x-ray induced radiative and nonradiative core-hole decay processes in thin films and solids. Tartu, 2008.
57. **Vadim Boltrushko.** Theory of vibronic transitions with strong nonlinear vibronic interaction in solids. Tartu, 2008.
58. **Andi Hektor.** Neutrino Physics beyond the Standard Model. Tartu, 2008.
59. **Raavo Josepson.** Photoinduced field-assisted electron emission into gases. Tartu, 2008.
60. **Martti Pärs.** Study of spontaneous and photoinduced processes in molecular solids using high-resolution optical spectroscopy. Tartu, 2008.
61. **Kristjan Kannike.** Implications of neutrino masses. Tartu, 2008.
62. **Vigen Issahhanjan.** Hole and interstitial centres in radiation-resistant MgO single crystals. Tartu, 2008.
63. **Veera Krasnenko.** Computational modeling of fluorescent proteins. Tartu, 2008.
64. **Mait Müntel.** Detection of doubly charged higgs boson in the CMS detector. Tartu, 2008.
65. **Kalle Kepler.** Optimisation of patient doses and image quality in diagnostic radiology. Tartu, 2009.
66. **Jüri Raud.** Study of negative glow and positive column regions of capillary HF discharge. Tartu, 2009.
67. **Sven Lange.** Spectroscopic and phase-stabilisation properties of pure and rare-earth ions activated ZrO_2 and HfO_2. Tartu, 2010.
68. **Aarne Kasikov.** Optical characterization of inhomogeneous thin films. Tartu, 2010.

69. **Heli Valtna-Lukner.** Superluminally propagating localized optical pulses. Tartu, 2010.
70. **Artjom Vargunin.** Stochastic and deterministic features of ordering in the systems with a phase transition. Tartu, 2010.
71. **Hannes Liivat.** Probing new physics in e+e− annihilations into heavy particles via spin orientation effects. Tartu, 2010.
72. **Tanel Mullari.** On the second order relativistic deviation equation and its applications. Tartu, 2010.
73. **Aleksandr Lissovski.** Pulsed high-pressure discharge in argon: spectroscopic diagnostics, modeling and development. Tartu, 2010.
74. **Aile Tamm.** Atomic layer deposition of high-permittivity insulators from cyclopentadienyl-based precursors. Tartu, 2010.
75. **Janek Uin.** Electrical separation for generating standard aerosols in a wide particle size range. Tartu, 2011.
76. **Svetlana Ganina.** Hajusandmetega ülesanded kui üks võimalus füüsikaõppe efektiivsuse tõstmiseks. Tartu, 2011
77. **Joel Kuusk.** Measurement of top-of-canopy spectral reflectance of forests for developing vegetation radiative transfer models. Tartu, 2011.
78. **Raul Rammula**. Atomic layer deposition of HfO_2 – nucleation, growth and structure development of thin films. Tartu, 2011.
79. **Сергей Наконечный.** Исследование электронно-дырочных и интерстициал-вакансионных процессов в монокристаллах MgO и LiF методами термоактивационной спектроскопии. Тарту, 2011.
80. **Niina Voropajeva.** Elementary excitations near the boundary of a strongly correlated crystal. Tartu, 2011.
81. **Martin Timusk.** Development and characterization of hybrid electro-optical materials. Tartu, 2012, 106 p.
82. **Merle Lust.** Assessment of dose components to Estonian population. Tartu, 2012, 84 p.
83. **Karl Kruusamäe.** Deformation-dependent electrode impedance of ionic electromechanically active polymers. Tartu, 2012, 128 p.
84. **Liis Rebane.** Measurement of the $W \to \tau\nu$ cross section and a search for a doubly charged Higgs boson decaying to τ-leptons with the CMS detector. Tartu, 2012, 156 p.
85. **Jevgeni Šablonin.** Processes of structural defect creation in pure and doped MgO and NaCl single crystals under condition of low or super high density of electronic excitations. Tartu, 2013, 145 p.
86. **Riho Vendt**. Combined method for establishment and dissemination of the international temperature scale. Tartu, 2013, 108 p.
87. **Peeter Piksarv.** Spatiotemporal characterization of diffractive and non-diffractive light pulses. Tartu, 2013, 156 p.
88. **Anna Šugai.** Creation of structural defects under superhigh-dense irradiation of wide-gap metal oxides. Tartu, 2013, 108 p.

89. **Ivar Kuusik.** Soft X-ray spectroscopy of insulators. Tartu, 2013, 113 p.
90. **Viktor Vabson**. Measurement uncertainty in Estonian Standard Laboratory for Mass. Tartu, 2013, 134 p.
91. **Kaupo Voormansik.** X-band synthetic aperture radar applications for environmental monitoring. Tartu, 2014, 117 p.
92. **Deivid Pugal.** hp-FEM model of IPMC deformation. Tartu, 2014, 143 p.
93. **Siim Pikker.** Modification in the emission and spectral shape of photostable fluorophores by nanometallic structures. Tartu, 2014, 98 p.
94. **Mihkel Pajusalu**. Localized Photosynthetic Excitons. Tartu, 2014, 183 p.
95. **Taavi Vaikjärv.** Consideration of non-adiabaticity of the Pseudo-Jahn-Teller effect: contribution of phonons. Tartu, 2014, 129 p.